Multi-approach gravity field models from Swarm GPS data

Signal and error in the Swarm models up to 2021-09-30

Delft University of Technology (TU Delft)
Astronomical Institute of the University of Bern (AIUB)
Astronomical Institute Ondřejov (ASU)
Institute of Geodesy Graz (IfG)
Ohio State University (OSU)

Version 1.0
2022-02-11

Prepared and checked by
João Encarnação
Work Package Manager

Approved by
Pieter Visser
Project Manager

Contents

List of Figures

List of Tables

1 Version history

Version 1, 2022-02-11

- Validation of combined models version 09, from start of mission until 2021-09-30.

2 Introduction

We report some statistics of the individual and combined GFMs produced on the context of the *Multi-approach gravity field models from Swarm GPS data* project. The approach for combining individual gravity field solutions, i.e. those produced by the various partners mentioned in Section 3, is described in Section 4.1. The procedure and assumption used to derive the statistics is described in Section 4.2. Finally, the results are presented in Section 5.

This report does not intend to draw conclusions regarding the presented statistics, it is merely a descriptive document of the signal and error in the individual and combined Swarm GFMs. For this reason, the text in Section 5 is restricted to clarifying the quantities shown in the plots.

3 Source data

The individual gravity field solutions are produced by the institutes listed in Table 1.

Table 1 – Overview of the gravity field estimation approaches

Inst.	Approach	Reference
AIUB	Celestial Mechanics Approach	Jäggi et al. (2016)
ASU	Decorrelated Acceleration Approach	Bezděk et al. (2016)
IfG	Short-Arcs Approach	Zehentner and Mayer-Gürr (2016)
OSU	Improved Energy Balance Approach	Guo et al. (2015)

Additional details about the different gravity field approaches can be found in (Teixeira da Encarnação and Visser, 2017).

The version of the individual GFMs is listed in Table 2.

Table 2 – Versions of the GFMs, and the KOs used in their estimation, relevant to this report.

Gravity Field Model	version	Kinematic Orbit
AIUB	01	AIUB
ASU	02 – 03	IfG
IfG	03 – 07	IfG
OSU	02	AIUB
combined	09	N/A

The version numbers listed in Table 2 are relevant within the project and are reported so that it is possible to trace back the results presented in Section 5. Particular to the combined models, version 09 relates to the chosen combination strategy, as concluded from Teixeira da Encarnação and Visser (2019).

4 Methodology

4.1 Combination

The combination of the models is conducted at the level of the solutions considering weights derived from Variance Component Estimation (VCE). As demonstrated in Teixeira da Encarnação and Visser (2019), the combination at the level of Normal Equation (NEQ) disagreed more with GRACE/GRACE-FO, as a result of the vastly different amplitudes of formal errors.

The combination considers the complete degree range (degrees 2 to 40) but the VCE weights are derived from degrees 2-20. This approach addresses the very high errors above degree 20, which would otherwise drive the value of the weights.

It is feasible to determine the VCE weights because there are two time-series based on AIUB orbits (i.e. AIUB and OSU) and two time-series based on IfG orbits (i.e. IfG and ASU). Therefore the impact of the KOs on the solutions and on the VCE weights is balanced.

4.2 Validation

The validation is done by comparing the individual and combined solutions to a model estimated from the Release 6 (RL06) GRACE/GRACE-FO GFMs produced at Center for Space Research (CSR), considering all solutions available at the this document is produced. This models fits a degree 1 polynomial and a yearly, semi-yearly, S2, K1 and K2 periods to the GRACE/GRACE-FO time series; the time series produced on the basis of the parameters resulting from this regression are referred to as *GRACE/GRACE-FO climatological model*.

The $C_{2,0}$ coefficient in all solutions has been replaced by the weekly time series provided by Goddard Space Flight Center (GSFC) (Loomis, Rachlin and Luthcke, 2019).

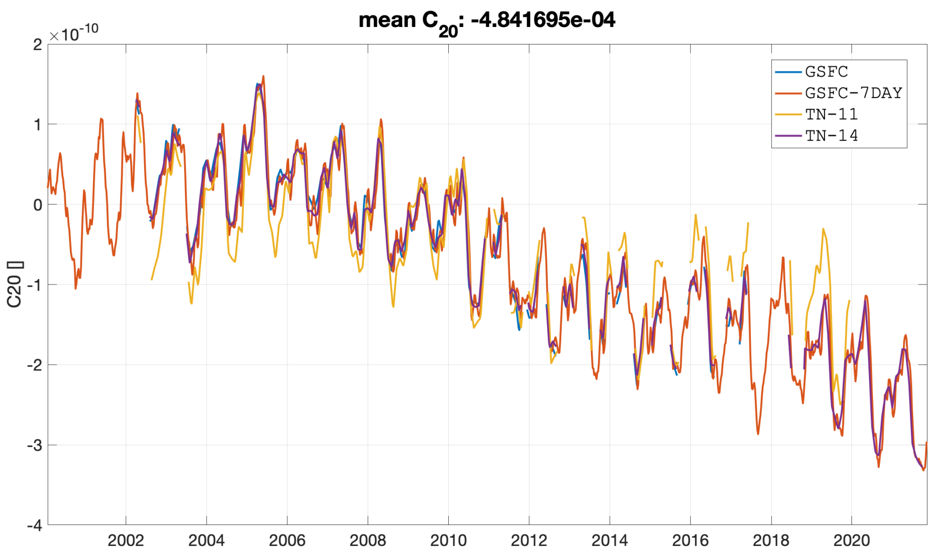

Figure 1 – Monthly (GSFC) and weekly (GSFC-7DAY) versions of the time series of SLR-derived C_{20} from Loomis, Rachlin and Luthcke (2019), compared to Cheng and Ries (2018) (TN-11) and Loomis and Rachlin (2020) (TN-14).

All solutions undergo a 750km radius spherical cap Gaussian filtering, unless otherwise noted, to clearly show the geophysical signal contained in the Swarm solutions. The GRACE and GOCE Gravity Model 05 (GGM05G) (Bettadpur et al., 2015) static GFM is subtracted from all models in order to isolate the time-variable component of Earth's gravity field. We chose to show the gravity field in terms of EWH, except for the statistics related to the correlation coefficient, which are non-dimensional as usual. The GRACE/GRACE-FO gravity field time series is linearly interpolated to the mid-month epoch of the Swarm solutions. The GRACE/GRACE-FO climatological model is evaluated at the same time domain. The analysis spans 2016-01-01 until 2021-09-30.

Some analyses are restricted to either the land or ocean areas. In those cases, the land or ocean mask is applied in the spatial domain and a Spherical Harmonic (SH) analysis is done on the masked grid. The ocean mask excludes the coastal ocean areas that are roughly 1000km or less from land areas, as shown in Figure 2, while the land mask has no buffer zone.

In Section 5.5, the geophysical signal represented by the Swarm solutions is evaluated on the basis of the time series of average EWH over restricted geographical locations, shown in Figure 3.

Each averaging is done over the corresponding spatial truncation of an equiangular grid representation of the SH coefficients. The locations shown in Sections 5.5.1 to 5.5.18 are related to the largest hydrological basins and polar regions with the highest signal variability

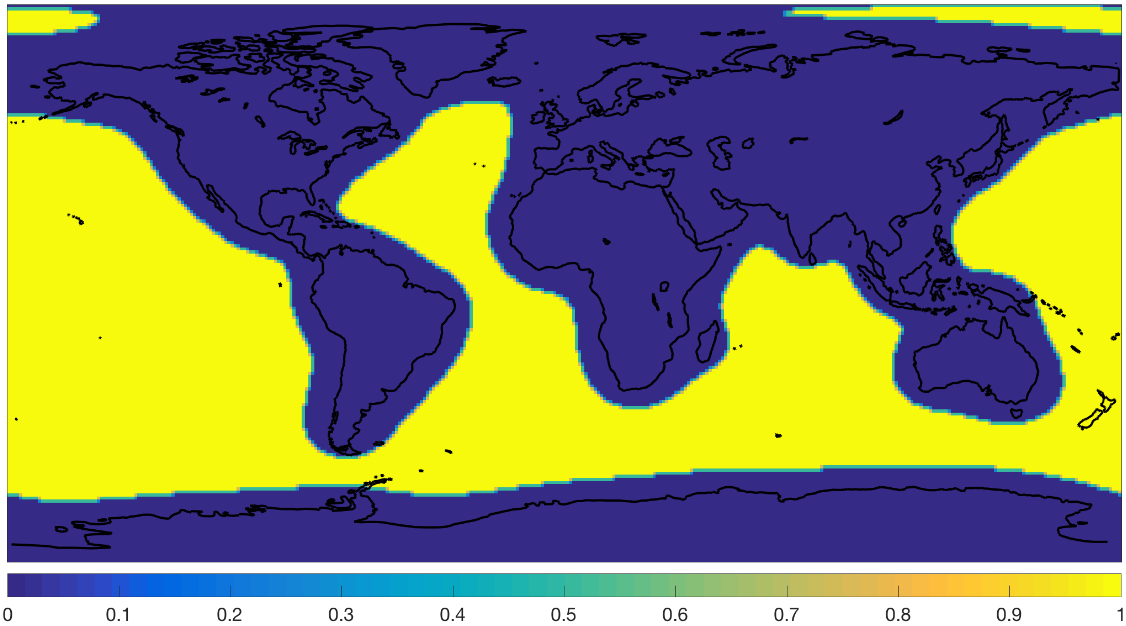

Figure 2 – Deep ocean mask.

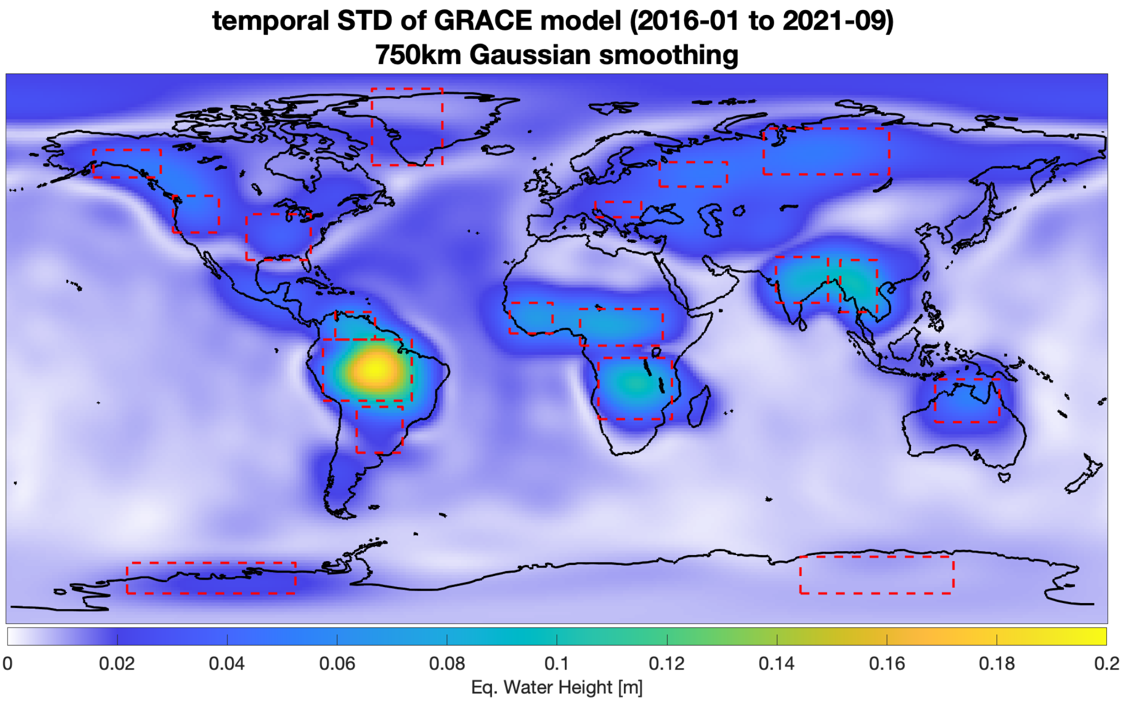

Figure 3 – Temporal variability of the GRACE/GRACE-FO climatological model, including the boundaries of the regions analysed in Section 5.5.1 to Section 5.5.18.

observed by GRACE/GRACE-FO. Note that there is no effort to meticulously consider or implement proper leakage reduction methods, e.g. by Guo, Duan and Shum (2010). We perform a parametric regression on all time series considering a constant and drift terms, along with annual and semi-annual sine and co-sine terms to improve the robustness. We plot the linear part of this regression, in order to quantify the accuracy of Swarm-derived climatological trends. The time series are plotted along with tables presenting some statistics. The values of the constant and linear terms for the Swarm and GRACE/GRACE-FO solutions (column 1) are show in terms of EWH (columns 2 and 4). Additionally, the difference of these parameters between the Swarm and GRACE/GRACE-FO solutions relative to the GRACE/GRACE-FO climatological model is listed in columns 3 and 5 (the values for the latter data set in these columns is zero). Finally, the correlation coefficients is presented in the last column (the value for GRACE/GRACE-FO climatological model is 1). The constant term is the average basin storage over the relevant data period.

5 Results

5.1 Spatial analysis

5.1.1 Degree-mean RMS difference

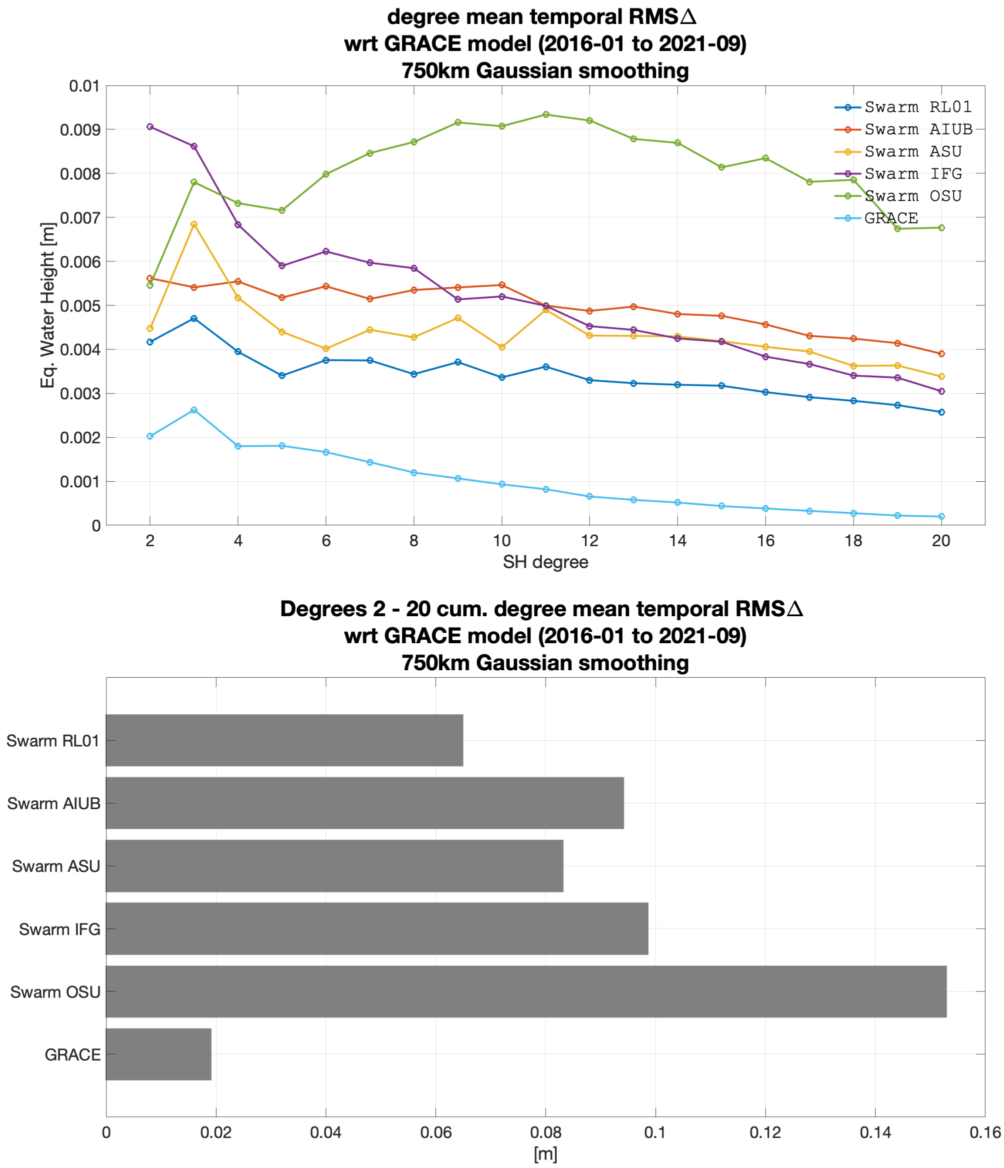

Figure 4 – Per-degree mean of the RMS difference (top) and cumulative degree-mean temporal RMS difference (bottom) between the Swarm GFMs and GRACE-based prediction, considering 750km Gaussian smoothing. This is (an estimate of) the average per-degree quality of the various Swarm solutions in the spectral domain (top) and globally (bottom) . The degree amplitudes remain relatively constant with increasing degree, instead of growing in terms of EWH, as the result of the smoothing.

5.1.2 Cumulative degree amplitude difference over land

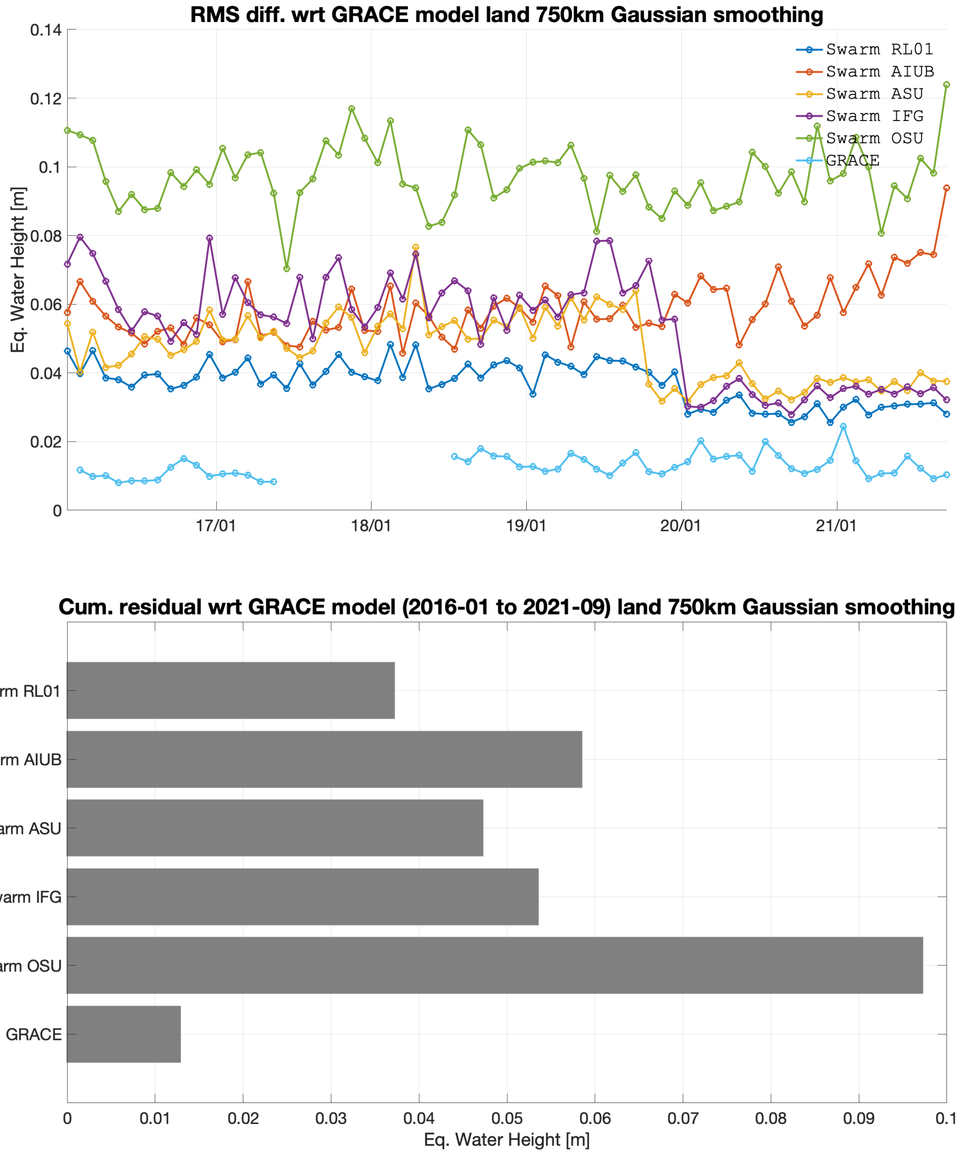

Figure 5 – Epoch-wise cumulative spatial RMS (top) and its global average (bottom) of the difference between Swarm GFMs and GRACE-based prediction, over land areas, considering 750km Gaussian smoothing. This is (an estimate of) the evolution of the ability of the various Swarm solutions to predict land mass transport processes over time (top) and its global sum (bottom).

5.1.3 Cumulative degree amplitude difference over oceans

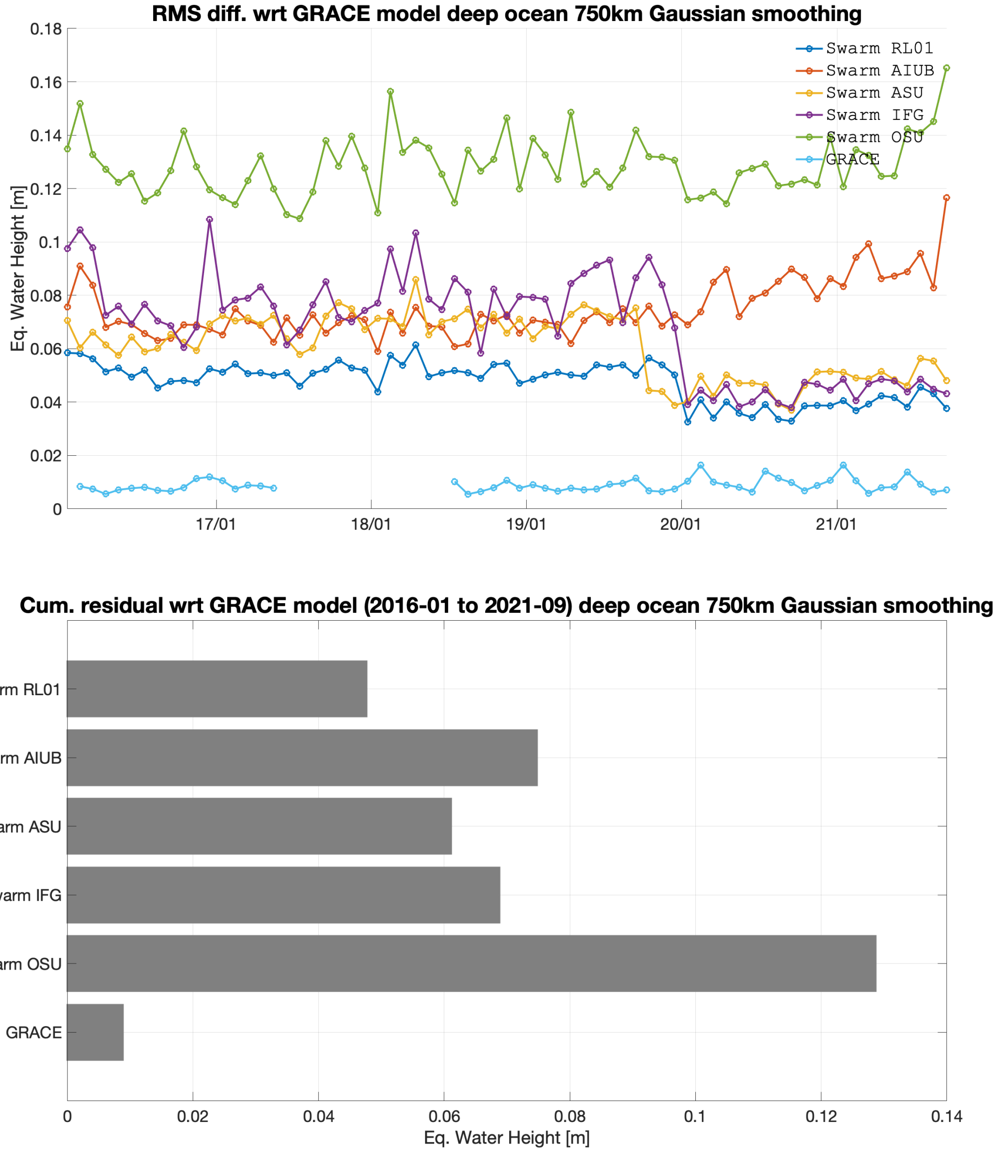

Figure 6 – Epoch-wise cumulative spatial RMS (top) and its global sum (bottom) of the difference between Swarm GFMs and GRACE-based prediction, over ocean areas, considering 750km Gaussian smoothing. This is the epoch-wise quality of the Swarm GFMs, and reported in the header of the combined GFMs files.

5.2 Temporal analysis

5.2.1 Per-degree mean correlation coefficient over land

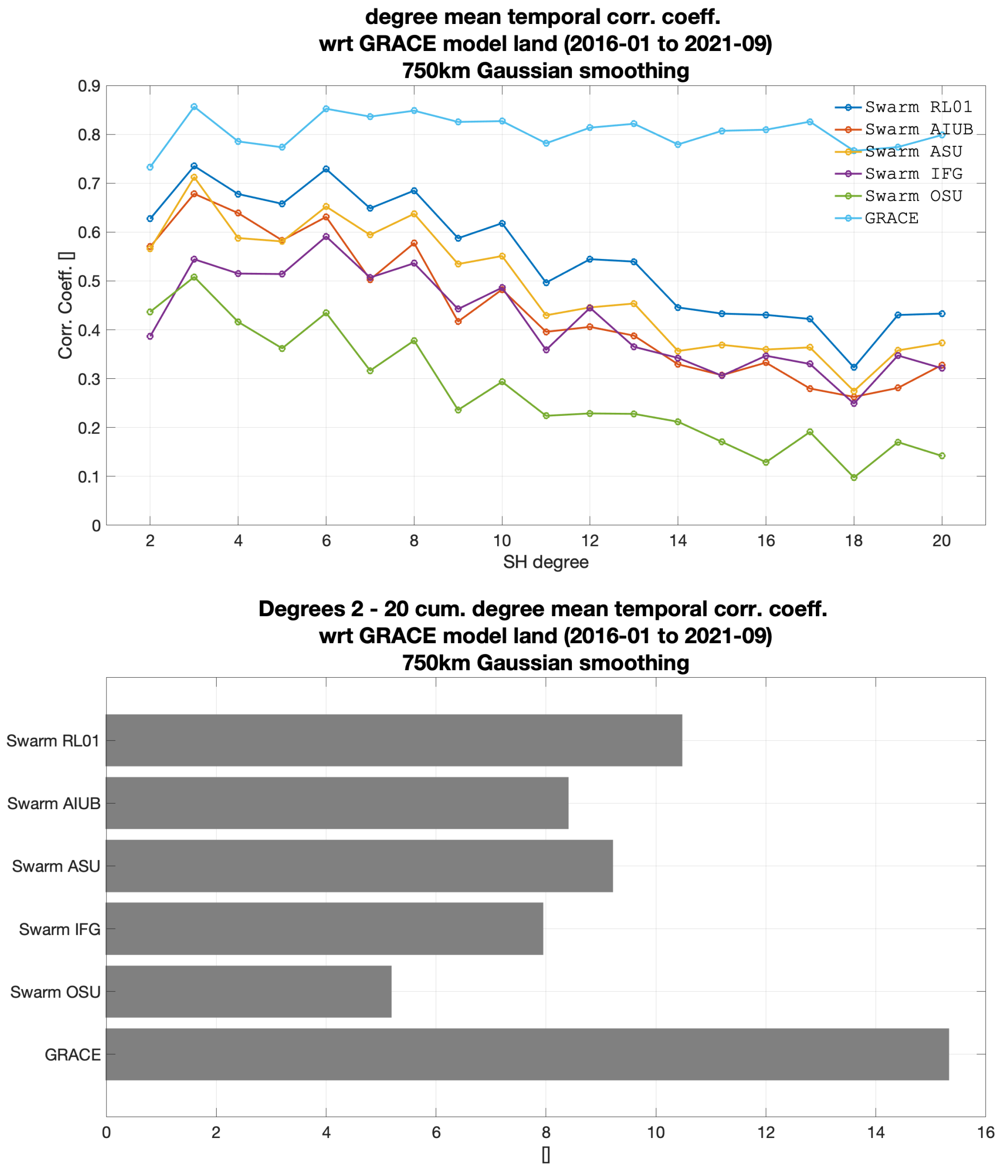

Figure 7 – Per-degree mean (top) and its overall cumulative (bottom) of the correlation coefficient between Swarm GFMs and GRACE-based prediction, over land areas, considering 750km Gaussian smoothing. The temporal correlation at every Stokes coefficient is computed and the average over each degree is plotted at the top. It illustrates how well the temporal variations of the Swarm models agree with what is predicted from the GRACE/GRACE-FO climatological model.

5.2.2 Per-degree mean correlation coefficient over oceans

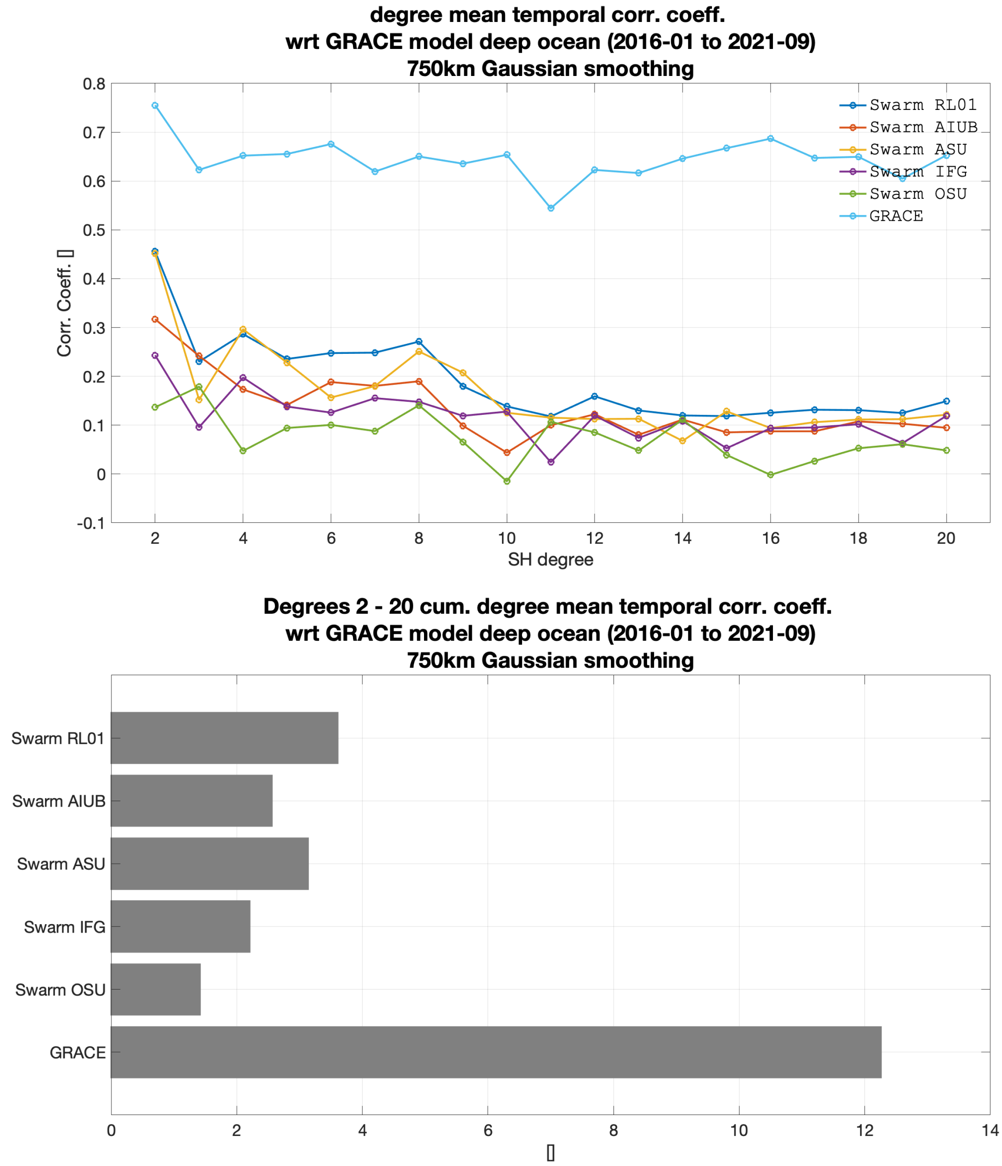

Figure 8 – Per-degree mean (top) and its overall cumulative (bottom) of the correlation coefficient between Swarm GFMs and GRACE-based prediction, over ocean areas, considering 750km Gaussian smoothing. It illustrates that the Swarm models agree poorly with the mass variations over the ocean as predicted by the GRACE/GRACE-FO climatological model.

5.2.3 Global unsmoothed per-degree mean correlation coefficient

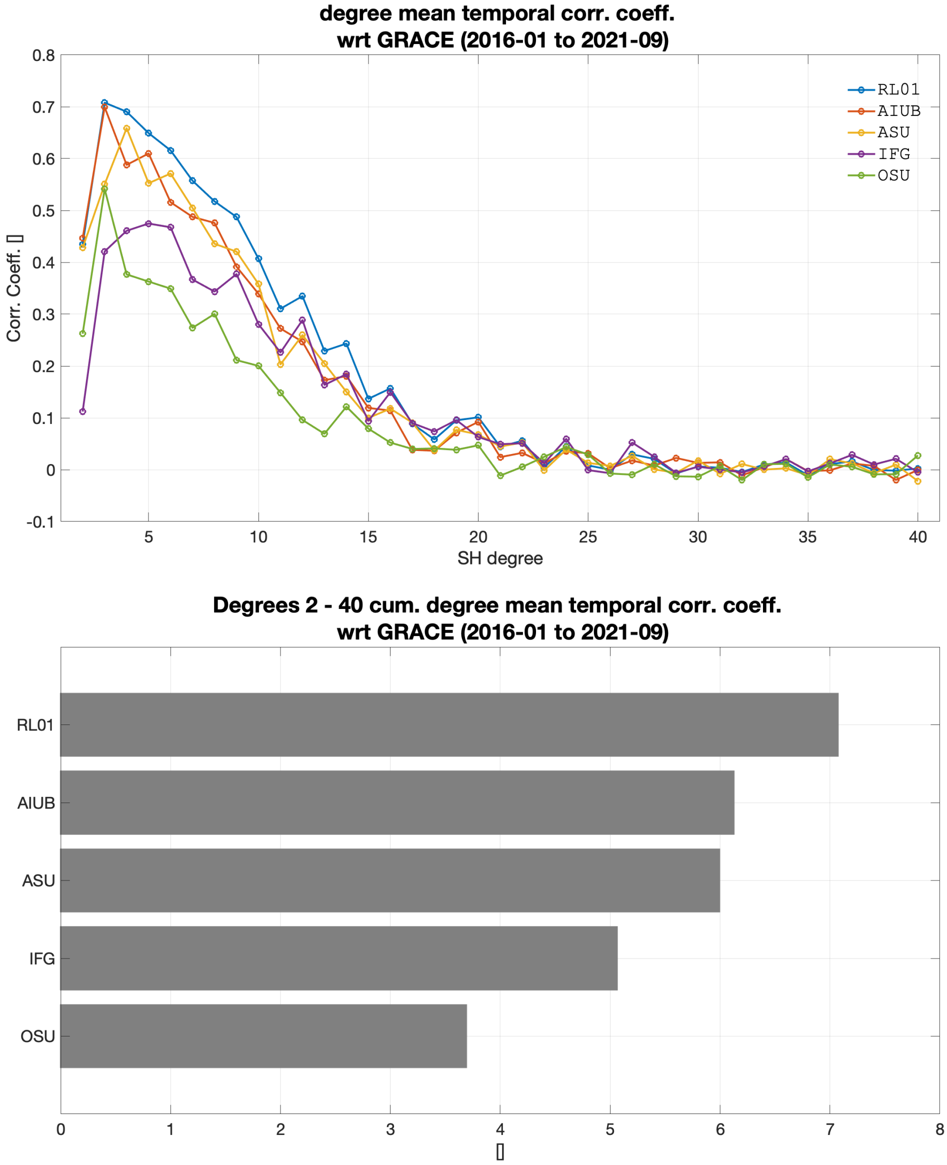

Figure 9 – Per-degree mean (top) and its overall cumulative (bottom) of the correlation coefficient between Swarm and GRACE/GRACE-FO GFMs (not the GRACE/GRACE-FO climatological model), globally and with no smoothing. It illustrates that the Swarm models fail to represent the same temporal variations as GRACE/GRACE-FO above degree 15-20.

5.2.4 Triangular plots of the RMS differences

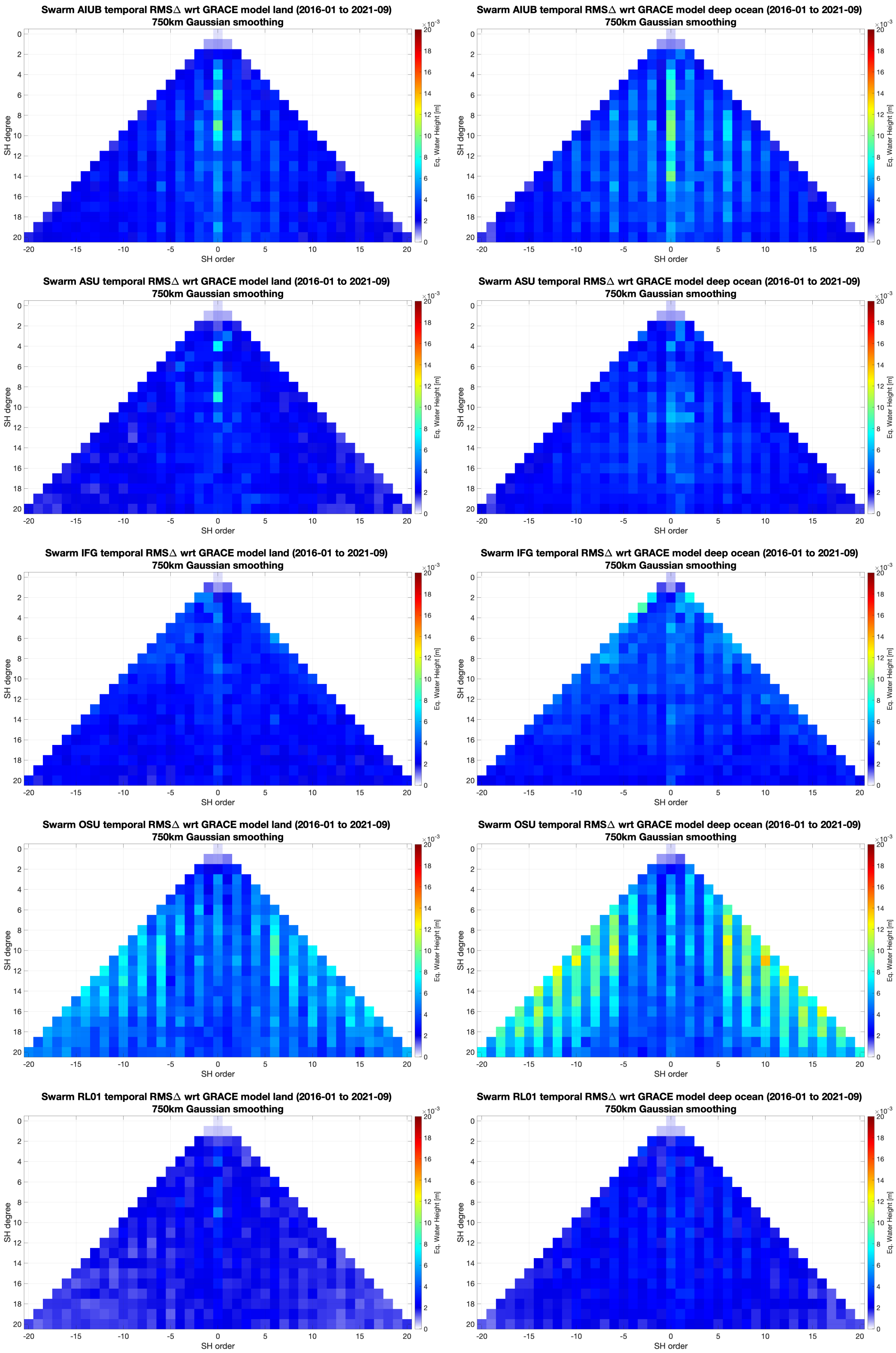

Figure 10 – Per-coefficient RMS difference between Swarm GFMs and GRACE-based prediction considering 750km Gaussian smoothing, over land (left column) and ocean (right column) areas, for AIUB, ASU, IfG, OSU and combined solutions (respectively from top to bottom).

5.3 Low-degree zonal coefficients

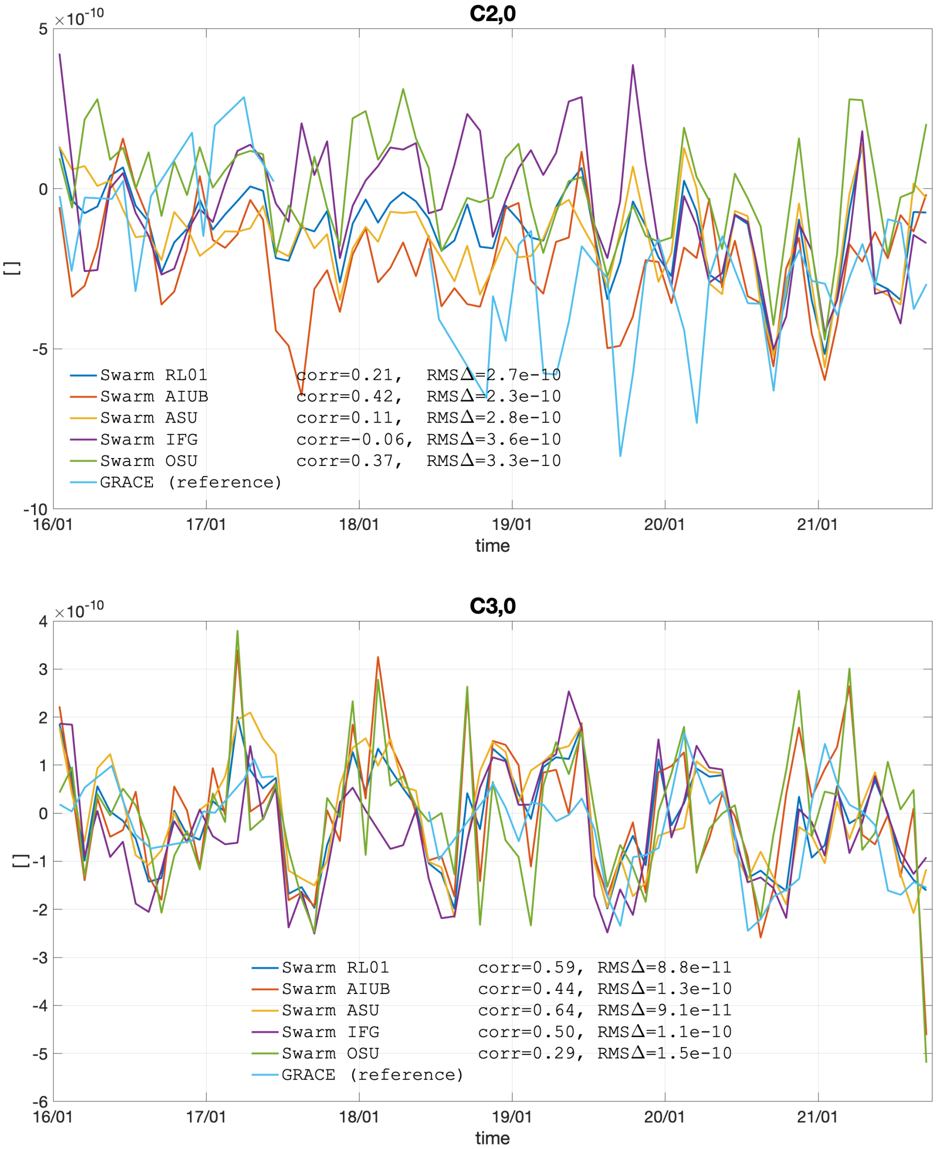

Figure 11 – Time series of the C_{20} (top) and C_{30} (bottom) coefficients, showing coefficients in the Swarm and GRACE/GRACE-FO GFMs.

5.4 Monthly models

5.4.1 Monthly degree-RMS

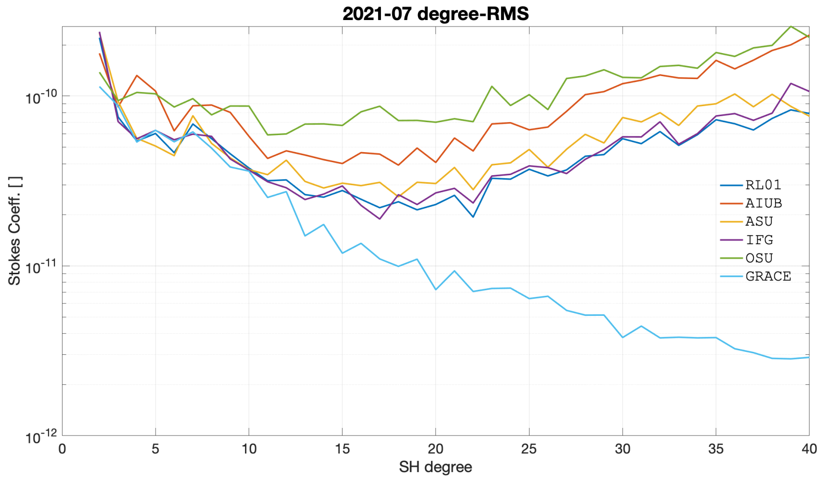

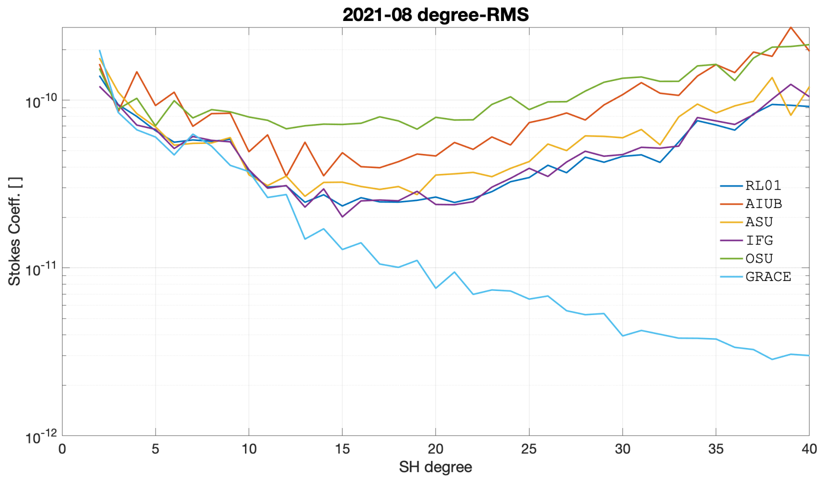

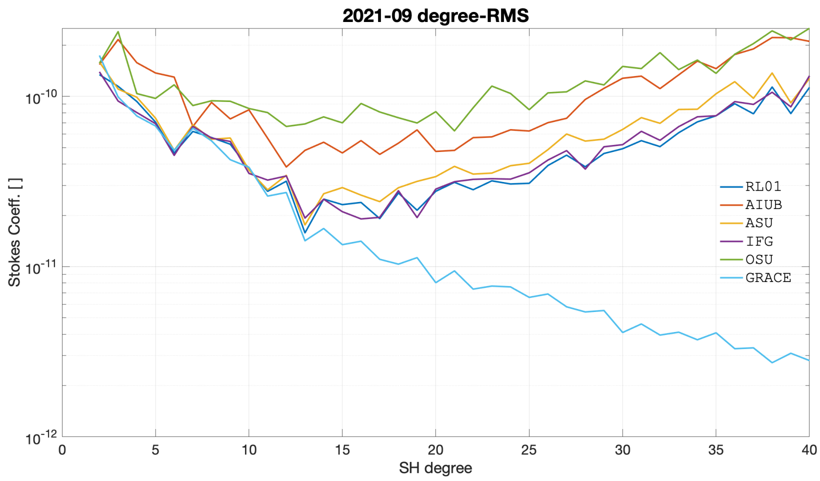

Figure 12 – Monthly degree-RMS for the 3 most recent months, all individual and combined Swarm solutions, as well as GRACE/GRACE-FO (no smoothing).

5.5 Time series of storage catchments

5.5.1 Amazon basin

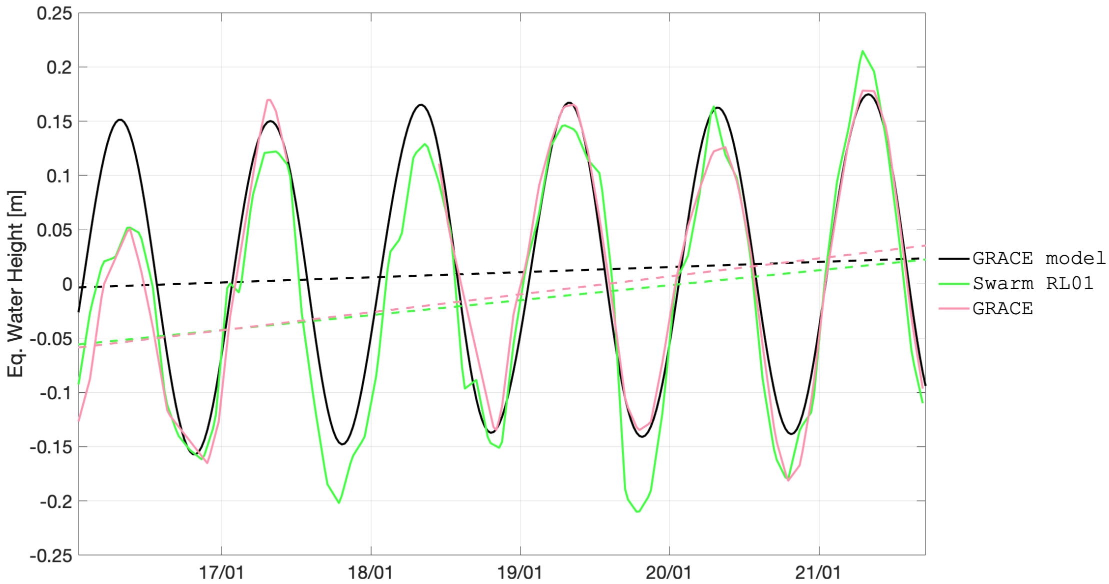

Figure 13 – Time series of EWH for the Amazon basin (latitude -17 to 3 degrees, longitude -76 to -47 degrees).

solution	constant term [cm]	constant term Δ [cm]	linear term [cm/year]	linear term Δ [cm/year]	corr. coeff. [ ]
GRACE MODEL	1.58	0.00	0.47	0.00	1.00
Swarm RL01	-1.07	-2.65	1.38	0.90	0.95
GRACE	1.16	-0.43	1.66	1.18	0.93

Table 3 – Statistics of the agreement between GRACE/GRACE-FO and Swarm time series relative to the GRACE/GRACE-FO climatological model for the Amazon basin.

5.5.2 Orinoco basin

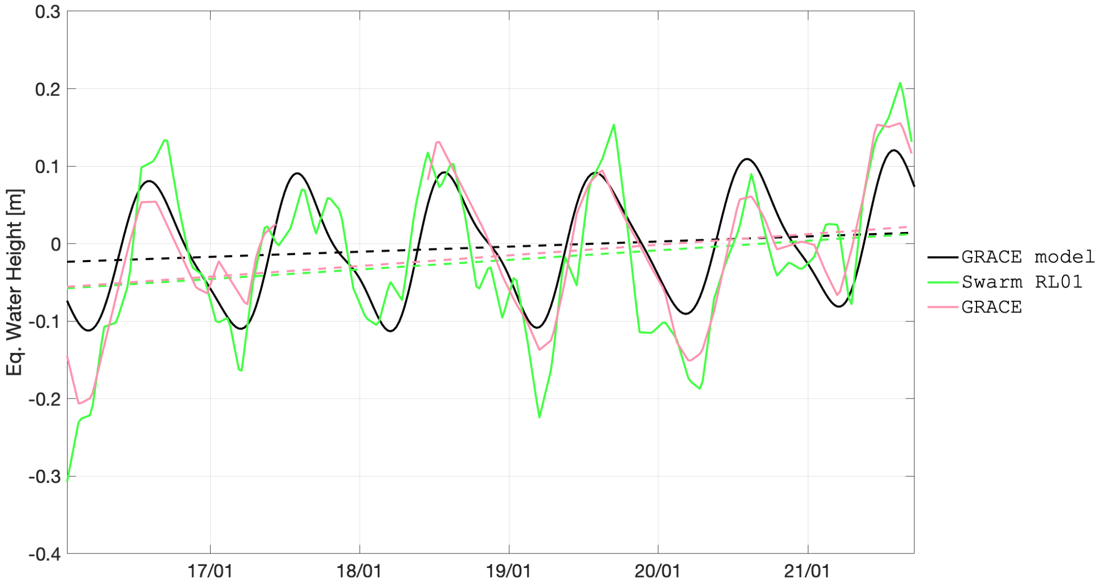

Figure 14 – Time series of EWH for the Orinoco basin (latitude -3 to 12 degrees, longitude -72 to -59 degrees).

solution	constant term [cm]	constant term Δ [cm]	linear term [cm/year]	linear term Δ [cm/year]	corr. coeff. [ ]
GRACE MODEL	-0.47	0.00	0.66	0.00	1.00
Swarm RL01	-2.28	-1.81	1.24	0.58	0.81
GRACE	-1.27	-0.80	1.37	0.71	0.88

Table 4 – Statistics of the agreement between GRACE/GRACE-FO and Swarm time series relative to the GRACE/GRACE-FO climatological model for the Orinoco basin.

5.5.3 La Plata basin

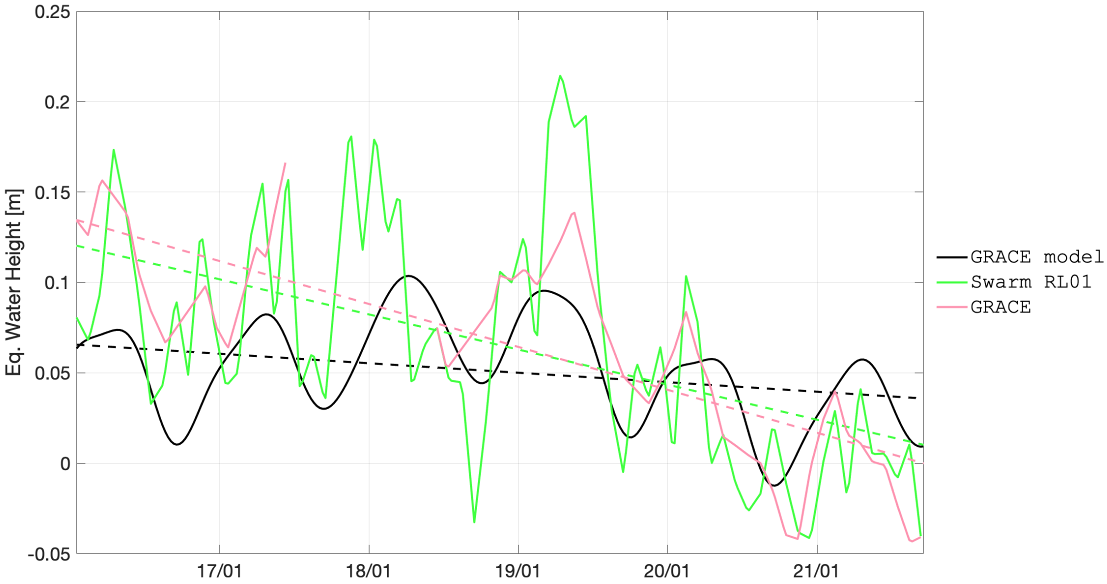

Figure 15 – Time series of EWH for the La Plata basin (latitude -34 to -19 degrees, longitude -65 to -50 degrees).

solution	constant term [cm]	constant term Δ [cm]	linear term [cm/year]	linear term Δ [cm/year]	corr. coeff. [ ]
GRACE MODEL	5.14	0.00	-0.52	0.00	1.00
Swarm RL01	6.56	1.42	-1.94	-1.42	0.66
GRACE	6.11	0.97	-2.37	-1.85	0.74

Table 5 – Statistics of the agreement between GRACE/GRACE-FO and Swarm time series relative to the GRACE/GRACE-FO climatological model for the La Plata basin.

5.5.4 Mississippi basin

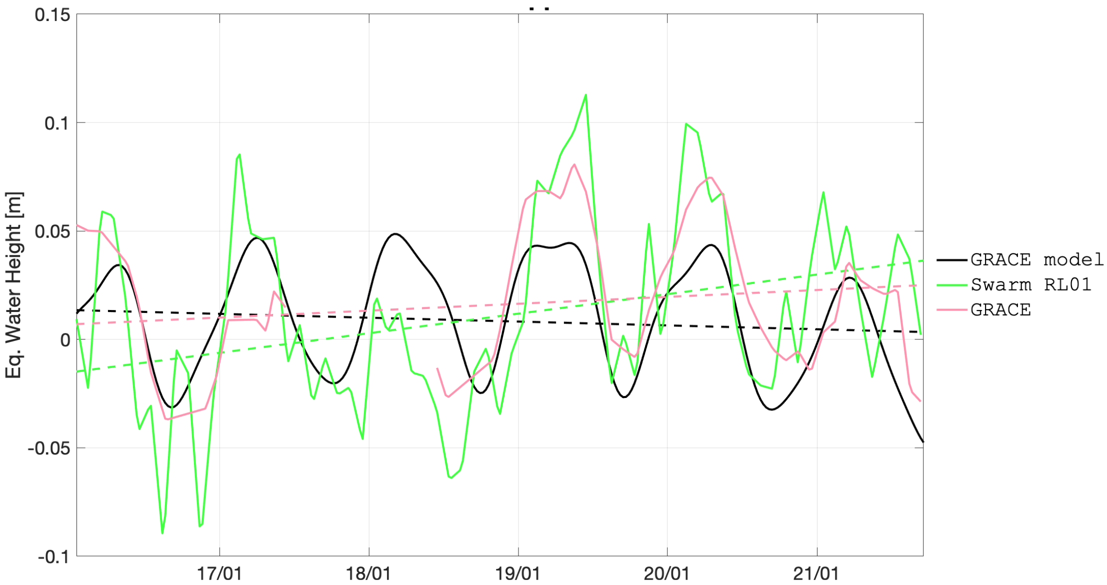

Figure 16 – Time series of EWH for the Mississippi basin (latitude 29 to 44 degrees, longitude -101 to -80 degrees).

solution	constant term [cm]	constant term Δ [cm]	linear term [cm/year]	linear term Δ [cm/year]	corr. coeff. [ ]
GRACE MODEL	0.91	0.00	-0.18	0.00	1.00
Swarm RL01	1.19	0.27	0.90	1.08	0.55
GRACE	2.05	1.14	0.32	0.49	0.77

Table 6 – Statistics of the agreement between GRACE/GRACE-FO and Swarm time series relative to the GRACE/GRACE-FO climatological model for the Mississippi basin.

5.5.5 Columbia region

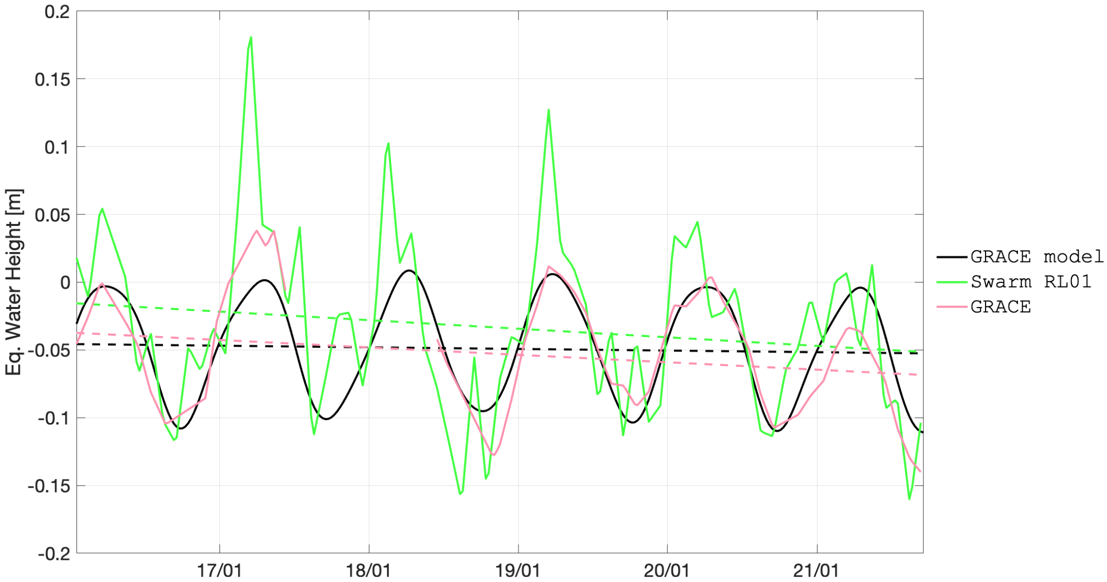

Figure 17 – Time series of EWH for the Columbia region (latitude 38 to 50 degrees, longitude -125 to -110 degrees).

solution	constant term [cm]	constant term Δ [cm]	linear term [cm/year]	linear term Δ [cm/year]	corr. coeff. [ ]
GRACE MODEL	-4.77	0.00	-0.12	0.00	1.00
Swarm RL01	-3.18	1.59	-0.63	-0.51	0.77
GRACE	-4.99	-0.22	-0.55	-0.43	0.90

Table 7 – Statistics of the agreement between GRACE/GRACE-FO and Swarm time series relative to the GRACE/GRACE-FO climatological model for the Columbia region.

5.5.6 Alaska

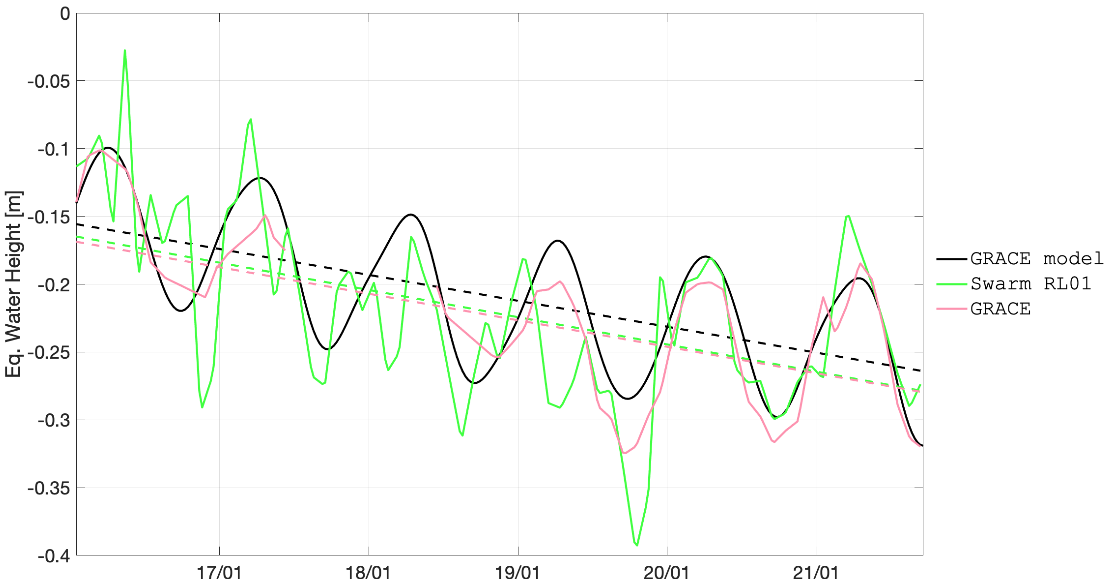

Figure 18 – Time series of EWH for the Alaska (latitude 56 to 65 degrees, longitude -151 to -129 degrees).

solution	constant term [cm]	constant term Δ [cm]	linear term [cm/year]	linear term Δ [cm/year]	corr. coeff. [ ]
GRACE MODEL	-20.85	0.00	-1.91	0.00	1.00
Swarm RL01	-22.03	-1.18	-2.01	-0.10	0.76
GRACE	-22.57	-1.72	-1.96	-0.04	0.95

Table 8 – Statistics of the agreement between GRACE/GRACE-FO and Swarm time series relative to the GRACE/GRACE-FO climatological model for the Alaska.

5.5.7 Western Greenland region

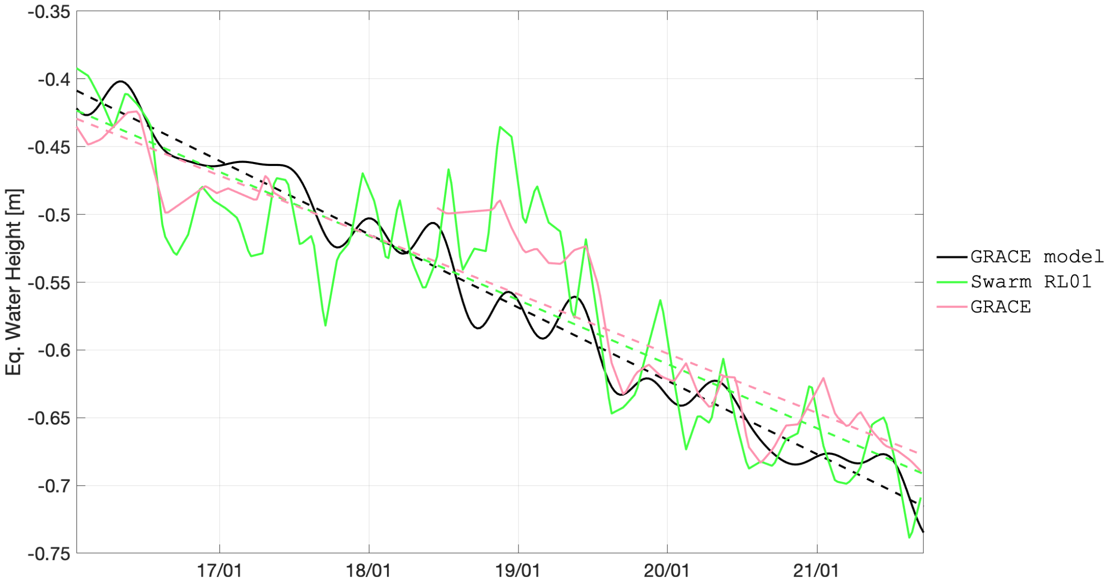

Figure 19 – Time series of EWH for the Western Greenland region (latitude 60 to 85 degrees, longitude -60 to -37 degrees).

solution	constant term [cm]	constant term Δ [cm]	linear term [cm/year]	linear term Δ [cm/year]	corr. coeff. [ ]
GRACE MODEL	-56.16	0.00	-5.41	0.00	1.00
Swarm RL01	-55.76	0.40	-4.73	0.68	0.90
GRACE	-56.72	-0.56	-4.38	1.03	0.95

Table 9 – Statistics of the agreement between GRACE/GRACE-FO and Swarm time series relative to the GRACE/GRACE-FO climatological model for the Western Greenland region.

5.5.8 Danube basin

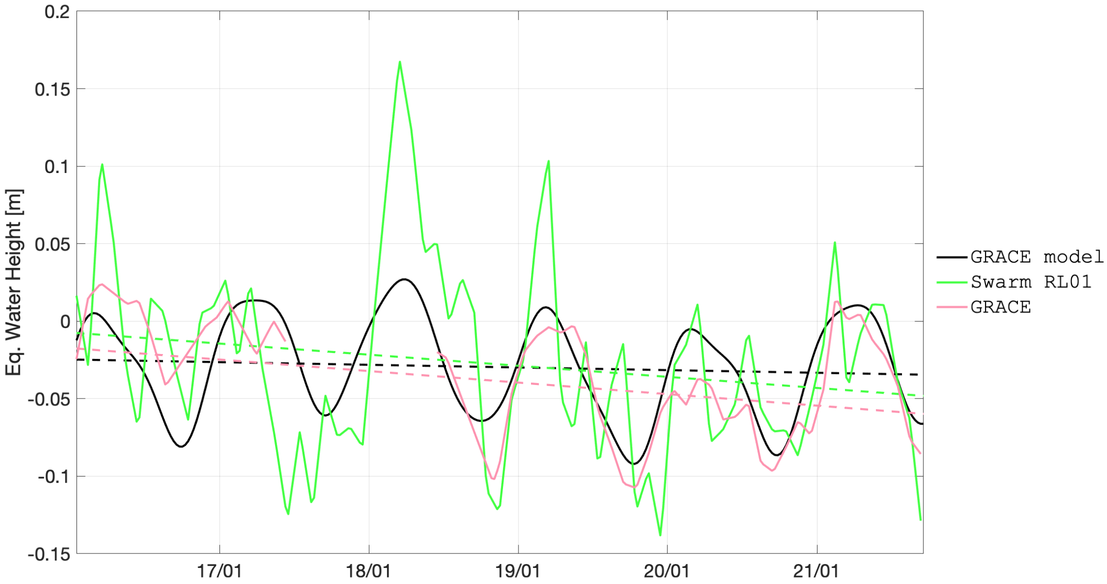

Figure 20 – Time series of EWH for the Danube basin (latitude 43 to 48 degrees, longitude 13 to 28 degrees).

solution	constant term [cm]	constant term Δ [cm]	linear term [cm/year]	linear term Δ [cm/year]	corr. coeff. [ ]
GRACE MODEL	-2.86	0.00	-0.17	0.00	1.00
Swarm RL01	-2.55	0.31	-0.72	-0.54	0.59
GRACE	-3.67	-0.81	-0.74	-0.57	0.77

Table 10 – Statistics of the agreement between GRACE/GRACE-FO and Swarm time series relative to the GRACE/GRACE-FO climatological model for the Danube basin.

5.5.9 Western Sub-Saharan basin

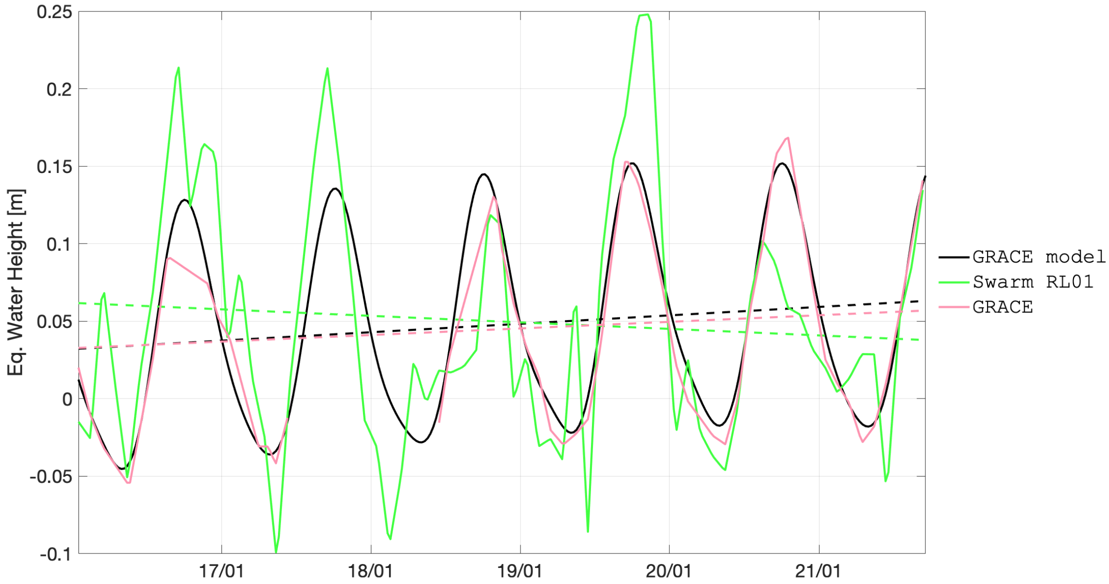

Figure 21 – Time series of EWH for the Western Sub-Saharan basin (latitude 5 to 15 degrees, longitude -15 to -1 degrees).

solution	constant term [cm]	constant term Δ [cm]	linear term [cm/year]	linear term Δ [cm/year]	corr. coeff. [ ]
GRACE MODEL	4.51	0.00	0.54	0.00	1.00
Swarm RL01	4.71	0.20	-0.42	-0.96	0.76
GRACE	3.60	-0.91	0.43	-0.12	0.98

Table 11 – Statistics of the agreement between GRACE/GRACE-FO and Swarm time series relative to the GRACE/GRACE-FO climatological model for the Western Sub-Saharan basin.

5.5.10 Eastern Sub-Saharan basin

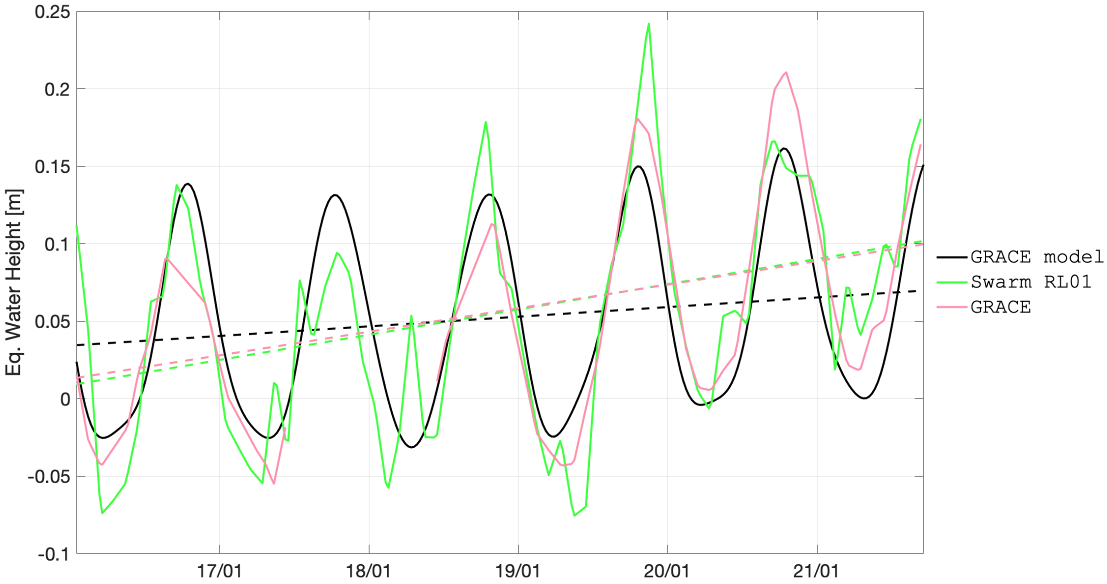

Figure 22 – Time series of EWH for the Eastern Sub-Saharan basin (latitude 1 to 13 degrees, longitude -8 to 35 degrees).

solution	constant term [cm]	constant term Δ [cm]	linear term [cm/year]	linear term Δ [cm/year]	corr. coeff. [ ]
GRACE MODEL	4.93	0.00	0.62	0.00	1.00
Swarm RL01	5.24	0.31	1.63	1.01	0.85
GRACE	5.26	0.33	1.52	0.90	0.92

Table 12 – Statistics of the agreement between GRACE/GRACE-FO and Swarm time series relative to the GRACE/GRACE-FO climatological model for the Eastern Sub-Saharan basin.

5.5.11 Congo and Zambezi basins

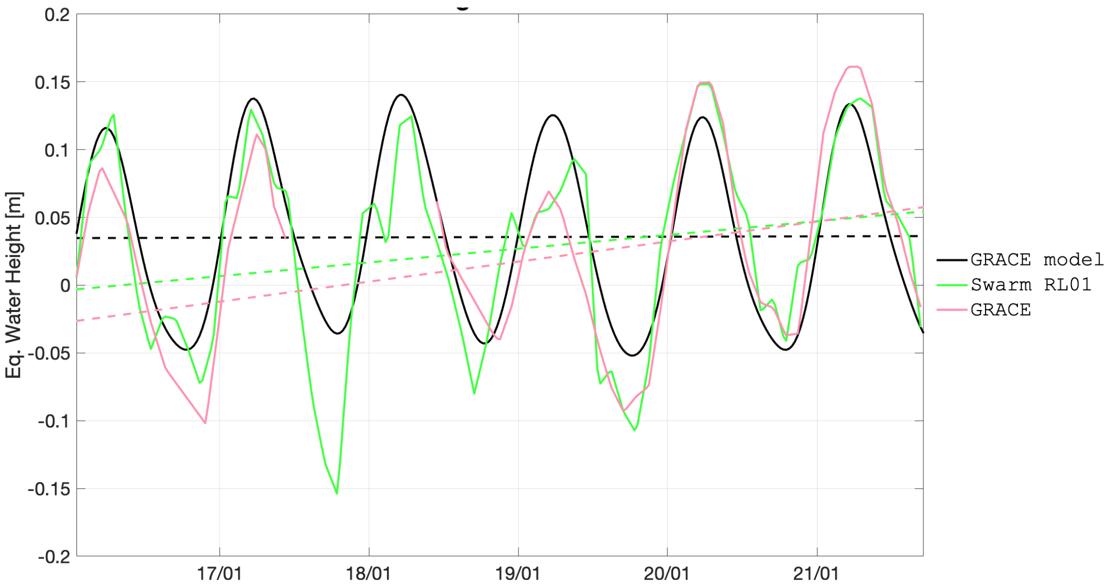

Figure 23 – Time series of EWH for the Congo and Zambezi basins (latitude -23 to -3 degrees, longitude 14 to 38 degrees).

solution	constant term [cm]	constant term Δ [cm]	linear term [cm/year]	linear term Δ [cm/year]	corr. coeff. [ ]
GRACE MODEL	3.80	0.00	0.03	0.00	1.00
Swarm RL01	2.83	-0.97	1.01	0.99	0.87
GRACE	2.96	-0.85	1.48	1.45	0.88

Table 13 – Statistics of the agreement between GRACE/GRACE-FO and Swarm time series relative to the GRACE/GRACE-FO climatological model for the Congo and Zambezi basins.

5.5.12 Volga basin

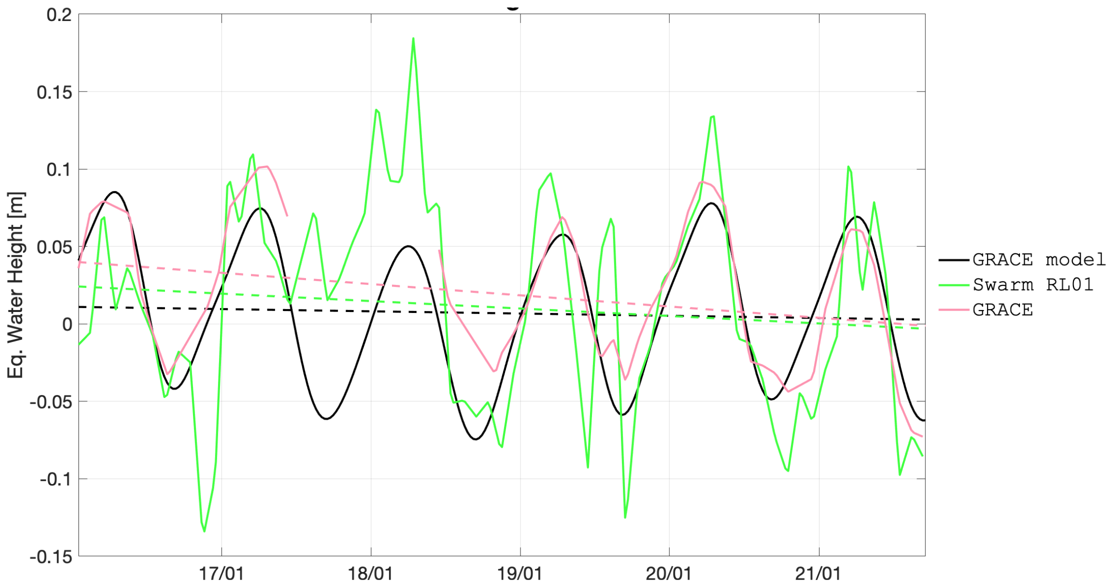

Figure 24 – Time series of EWH for the Volga basin (latitude 53 to 61 degrees, longitude 34 to 56 degrees).

solution	constant term [cm]	constant term Δ [cm]	linear term [cm/year]	linear term Δ [cm/year]	corr. coeff. [ ]
GRACE MODEL	0.81	0.00	-0.14	0.00	1.00
Swarm RL01	1.29	0.48	-0.48	-0.34	0.59
GRACE	2.13	1.33	-0.73	-0.58	0.89

Table 14 – Statistics of the agreement between GRACE/GRACE-FO and Swarm time series relative to the GRACE/GRACE-FO climatological model for the Volga basin.

5.5.13 Siberia region

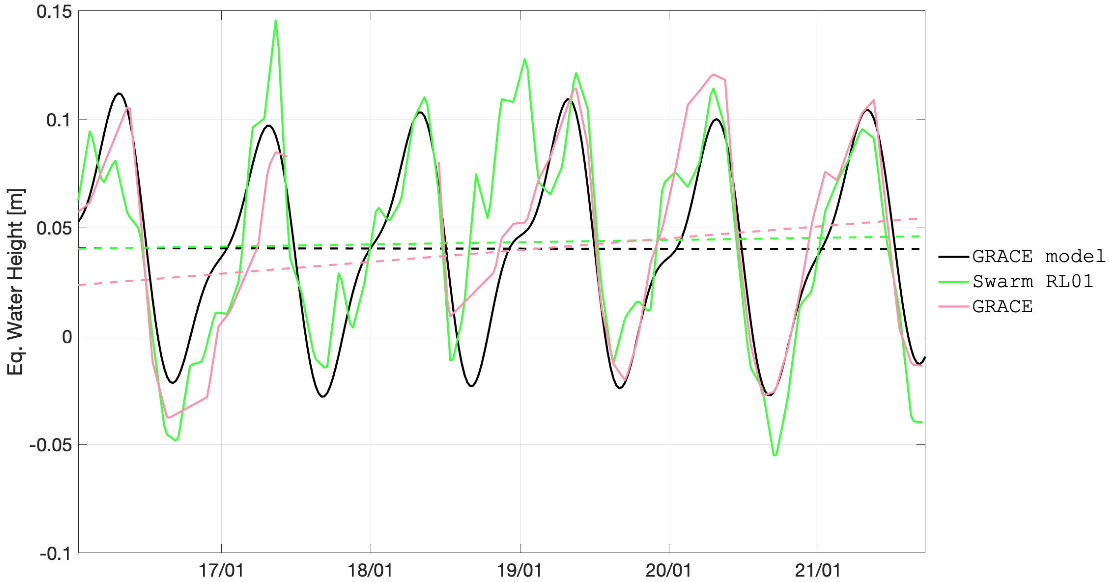

Figure 25 – Time series of EWH for the Siberia region (latitude 57 to 72 degrees, longitude 68 to 109 degrees).

solution	constant term [cm]	constant term Δ [cm]	linear term [cm/year]	linear term Δ [cm/year]	corr. coeff. [ ]
GRACE MODEL	4.13	0.00	-0.01	0.00	1.00
Swarm RL01	4.39	0.26	0.10	0.11	0.81
GRACE	4.72	0.59	0.55	0.55	0.89

Table 15 – Statistics of the agreement between GRACE/GRACE-FO and Swarm time series relative to the GRACE/GRACE-FO climatological model for the Siberia region.

5.5.14 Ganges-Brahmaputra basin

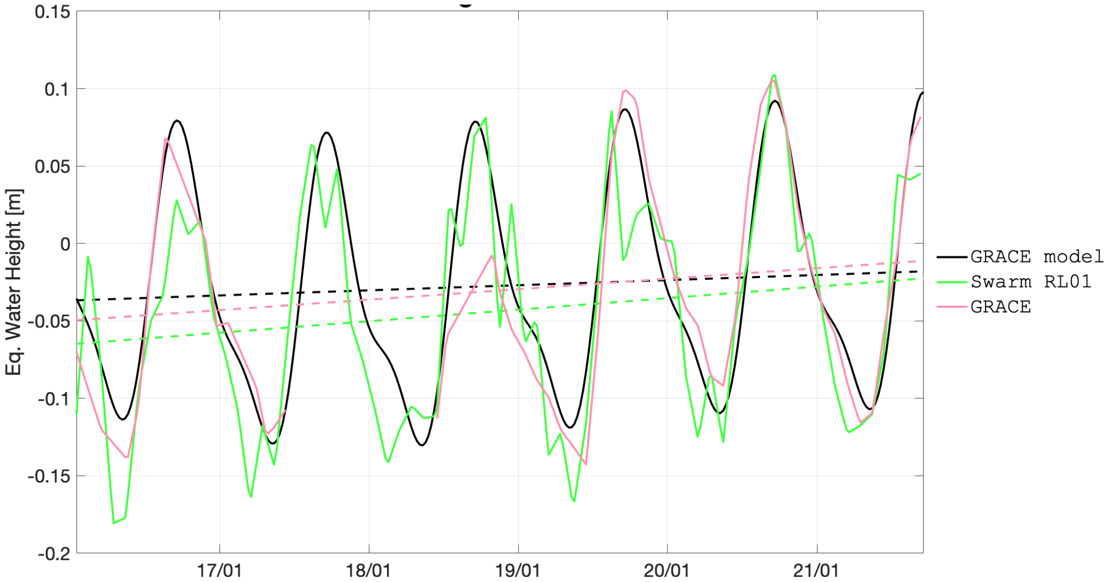

Figure 26 – Time series of EWH for the Ganges-Brahmaputra basin (latitude 15 to 30 degrees, longitude 72 to 89 degrees).

solution	constant term [cm]	constant term Δ [cm]	linear term [cm/year]	linear term Δ [cm/year]	corr. coeff. [ ]
GRACE MODEL	-2.93	0.00	0.33	0.00	1.00
Swarm RL01	-4.59	-1.65	0.74	0.42	0.89
GRACE	-3.92	-0.99	0.68	0.35	0.91

Table 16 – Statistics of the agreement between GRACE/GRACE-FO and Swarm time series relative to the GRACE/GRACE-FO climatological model for the Ganges-Brahmaputra basin.

5.5.15 Indochina region

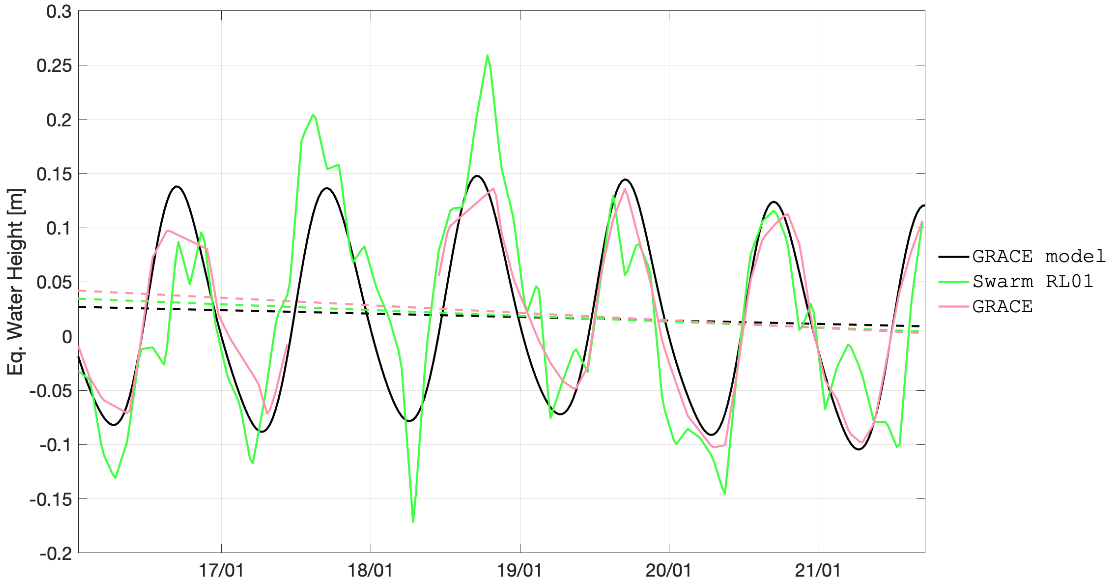

Figure 27 – Time series of EWH for the Indochina region (latitude 12 to 29 degrees, longitude 93 to 105 degrees).

solution	constant term [cm]	constant term Δ [cm]	linear term [cm/year]	linear term Δ [cm/year]	corr. coeff. [ ]
GRACE MODEL	1.58	0.00	-0.32	0.00	1.00
Swarm RL01	1.66	0.08	-0.53	-0.22	0.80
GRACE	0.98	-0.60	-0.69	-0.38	0.96

Table 17 – Statistics of the agreement between GRACE/GRACE-FO and Swarm time series relative to the GRACE/GRACE-FO climatological model for the Indochina region.

5.5.16 Northern Australia region

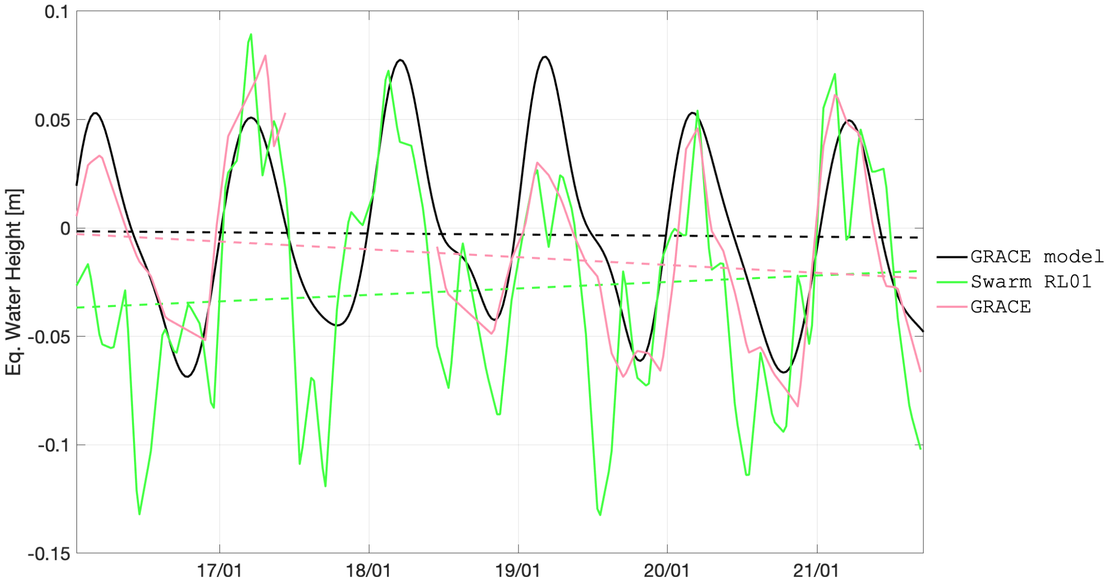

Figure 28 – Time series of EWH for the Northern Australia region (latitude -24 to -10 degrees, longitude 124 to 145 degrees).

solution	constant term [cm]	constant term Δ [cm]	linear term [cm/year]	linear term Δ [cm/year]	corr. coeff. [ ]
GRACE MODEL	-0.13	0.00	-0.05	0.00	1.00
Swarm RL01	-2.73	-2.60	0.30	0.35	0.68
GRACE	-1.00	-0.87	-0.36	-0.31	0.88

Table 18 – Statistics of the agreement between GRACE/GRACE-FO and Swarm time series relative to the GRACE/GRACE-FO climatological model for the Northern Australia region.

5.5.17 Western Antarctica region

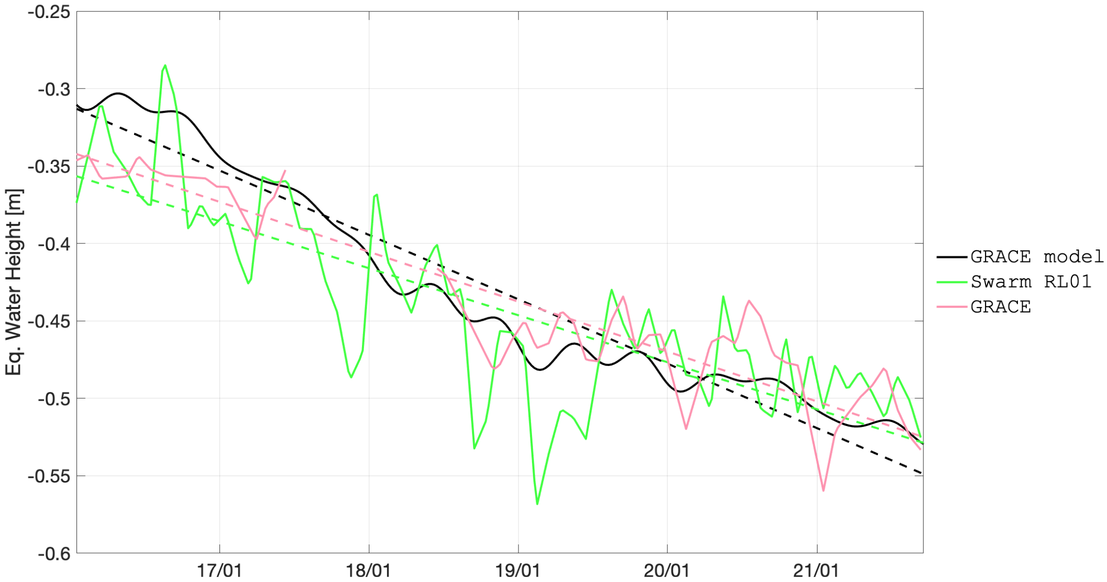

Figure 29 – Time series of EWH for the Western Antarctica region (latitude -80 to -70 degrees, longitude -140 to -85 degrees).

solution	constant term [cm]	constant term Δ [cm]	linear term [cm/year]	linear term Δ [cm/year]	corr. coeff. [ ]
GRACE MODEL	-43.09	0.00	-4.16	0.00	1.00
Swarm RL01	-44.21	-1.12	-3.04	1.12	0.87
GRACE	-44.51	-1.42	-3.22	0.94	0.96

Table 19 – Statistics of the agreement between GRACE/GRACE-FO and Swarm time series relative to the GRACE/GRACE-FO climatological model for the Western Antarctica region.

5.5.18 Eastern Antarctica region

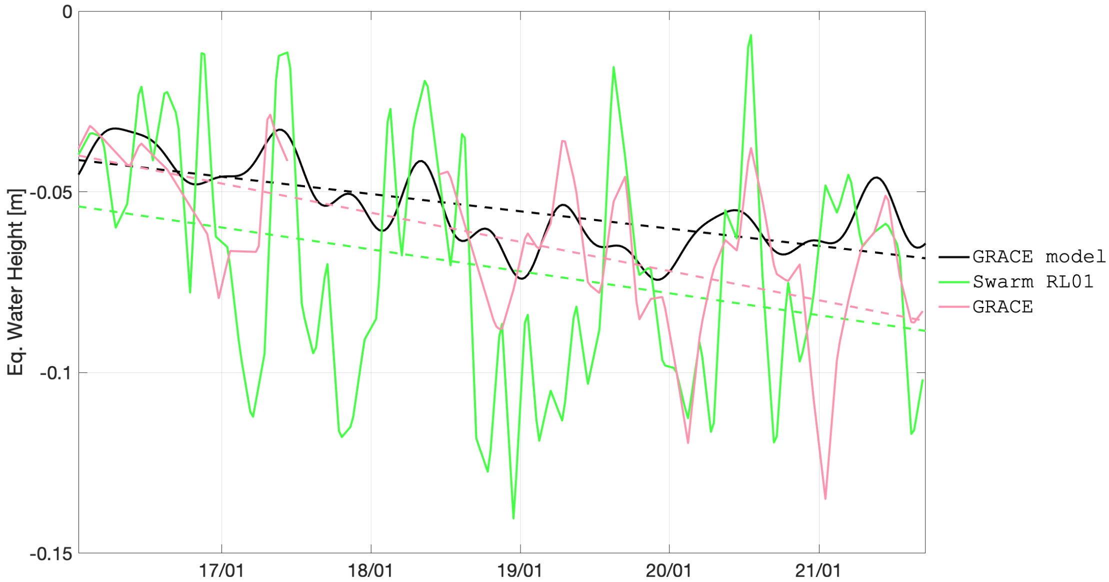

Figure 30 – Time series of EWH for the Eastern Antarctica region (latitude -80 to -68 degrees, longitude 80 to 130 degrees).

solution	constant term [cm]	constant term Δ [cm]	linear term [cm/year]	linear term Δ [cm/year]	corr. coeff. [ ]
GRACE MODEL	-5.45	0.00	-0.48	0.00	1.00
Swarm RL01	-7.07	-1.61	-0.61	-0.13	0.50
GRACE	-6.53	-1.08	-0.81	-0.33	0.65

Table 20 – Statistics of the agreement between GRACE/GRACE-FO and Swarm time series relative to the GRACE/GRACE-FO climatological model for the Eastern Antarctica region.

5.5.19 Overview

solution	constant term Δ RMS [cm]	linear term Δ RMS [cm/year]	corr. coeff. mean [ ]
GRACE model	0.00	0.00	1.00
Swarm RL01	1.32	0.75	0.76
GRACE	0.94	0.82	0.88

Table 21 – Statistics of the agreement between the GRACE and Swarm time series for the regions displayed in Sections 5.5.1 to 5.5.18.

5.6 Temporal variability

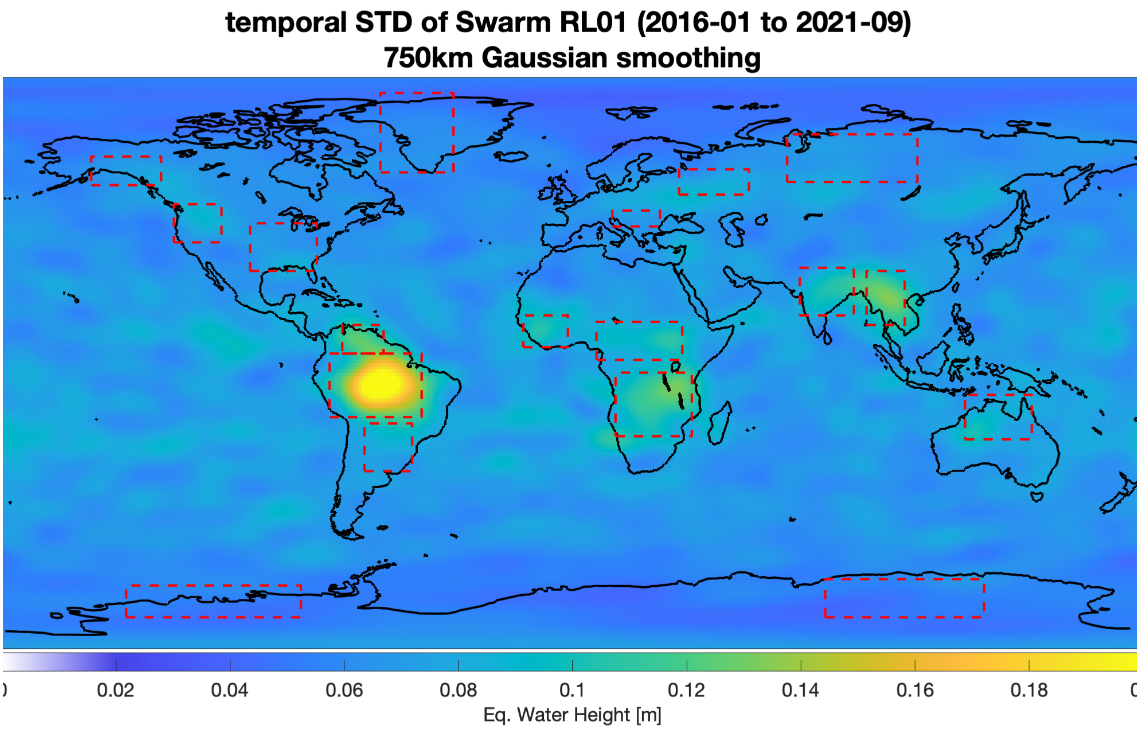

Figure 31 – Temporal variability of the Swarm combined solutions.

A Kinematic Orbits

A.1 Delft University of Technology

Software:	GPS High precision Orbit determination Software Tool (GHOST) (Helleputte, 2004; Wermuth, Montenbruck and Helleputte, 2010)
Preprocessing:	None
Differencing Scheme:	Undifferenced

Linear combination:	Ionosphere-free
Differential code bias:	N/A
Ionosphere model:	N/A
GPS observations:	Code and carrier phase
Carrier phase ambiguities:	Float
Estimator:	Bayesian weighted LS
Arc length:	30 hours
Observation weighting:	A-priori weights equal to 1m and 1mm for code and phase observations (resp.)
Data screening:	Minimum SNR of 10, minimum of 6 GPS satellites, code and phase outlier editing threshold of 2 m and 3.5 cm, respectively, 1 meter or larger difference between estimated KO positions and with Reduced-Dynamic PSO
Transmitter PCV:	Official IGS08 ANTEX (Schmid et al., 2007) up to day 17/028, official IGS14 ANTEX (Rebischung and Schmid, 2016) afterwards
Receiver PCV:	Empirically determined from stacking of reduced-dynamic POD residuals with 1° binning
GPS orbits and clocks:	Final orbits and 5 seconds clocks of CODE (Dach et al., 2017)
Earth precession model:	IAU 1976 (Lieske et al., 1977)
Earth nutation model:	IAU 1980 (Seidelmann, 1982)
Earth orientation model:	CODE final ERP

A.2 Astronomical Institute of the University of Bern

Software:	Bernese v5.3 (Dach et al., 2015)
Preprocessing:	Cycle slip detection based on epoch-difference solution
Differencing Scheme:	Undifferenced
Linear combination:	Ionosphere-free
Differential code bias:	N/A
Ionosphere model:	N/A
GPS observations:	Code and carrier phase
Carrier phase ambiguities:	Float up to 26 January 2020, ambiguity-fixed afterwards
Estimator:	Batch LS
Arc length:	24 hours
Observation weighting:	Constant
Data screening:	2 cm/s or larger time-differences of the geometry-free
Transmitter PCV:	Official IGS08 ANTEX (Schmid et al., 2007) up to day 17/028, official IGS14 ANTEX (Rebischung and Schmid, 2016) afterwards
Receiver PCV:	Stacking of carrier phase residuals from reduced-dynamic POD of approx. 120 days, 9 iterations, 1° binning linear combination of L1B GPS carrier phase observations
GPS orbits and clocks:	Final orbits and 5 seconds clocks of CODE (Dach et al., 2017)
Earth precession model:	IERS 2010 Conventions (Petit and Luzum, 2010)
Earth nutation model:	IERS 2010 Conventions (Petit and Luzum, 2010)
Earth orientation model:	CODE final ERP

A.3 Institute of Geodesy Graz

Software:	Gravity Recovery Object Oriented Programming System (GROOPS) (Mayer-gürr et al., 2020)

Preprocessing:	Cycle slip detection based on Melbourne-Wuebbena combination
Differencing Scheme:	Raw undifferenced
Linear combination:	None (the ionospheric influence is co-estimated)
Differential code bias:	Graz University of Technology (TUG) daily estimated absolute biases
Ionosphere model:	Slant total electron content (STEC) 1st, 2nd and 3rd order effects (Hoque and Jakowski, 2008) estimated in each epoch for each receiver-transmitter pair
GPS observations:	Code and carrier phase
Carrier phase ambiguities:	MLAMBDA (Chang, Yang and Zhou, 2005)
Estimator:	LS
Arc length:	24 hours
Observation weighting:	Elevation and azimuth-dependent, ROTI dependent
Data screening:	Implicit in VCE
Transmitter PCV:	Empirical, estimated from 5.5 years of data, including data from several LEO missions (GRACE, Jason 2 & 3, MetOp-A & -B, Sentinel 3A, Swarm, TanDEM-X, TerraSAR-X) (Zehentner, 2016)
Receiver PCV:	Empirical, spherical harmonics (maximum D/O 100), derived from 38 months of data
GPS orbits:	TUG, estimated using ≈ 200 daily IGS stations
GPS clocks:	TUG 30 seconds, interpolated using CODE 5 seconds finals to a sampling of 5 seconds
Earth precession model:	IAU 2006/2000A precession-nutation model (Coppola, Seago and Vallado, 2009)
Earth nutation model:	IAU 2006/2000A precession-nutation model (Coppola, Seago and Vallado, 2009)
Earth orientation model:	IERS EOP 08 C04 (Petit and Luzum, 2010)

A.4 Common

Receiver clock corrections:	Co-estimated
Phase wind-up:	Correction applied
Sampling rate:	10 seconds up to 15 July 2014, 1 seconds afterwards
Receiver antenna offset:	satellite specific values
Elevation cut-off angle:	0°
Swarm attitude:	L1B attitude data
GPS attitude model:	(Kouba, 2009)

B Gravity Field Models

B.1 Astronomical Institute of the University of Bern

Software:	Bernese v5.3 (Dach et al., 2015)
Approach:	Celestial Mechanics Approach (CMA) (Beutler et al., 2010)
Reference GFM:	AIUB-GRACE03S (Jäggi et al., 2011)
Empirical Parameters:	Daily and 15 minutes, both piecewise-constant (constrained)
Coord. Axis Combination:	TBD
Single Sat. Combination:	NEQ, equal weights

Temporal correlations: None
Drag Model: None
EARP and EIRP Models: None
Non-tidal Model: **Unti Nov 2017:**AOD1B (Flechtner, Schmidt and Meyer, 2006; Flechtner, 2007; Flechtner, 2011)
After Nov 2017:AOD1B-RL06 (Dobslaw et al., 2017)
Ocean Tidal Model: EOT11a (Savcenko and Bosch, 2012)
Permanent Tide System: tide-free

B.2 Astronomical Institute Ondřejov

Software: (developed in-house)
Approach: Decorrelated Acceleration Approach (DAA) (Bezděk et al., 2014; Bezděk et al., 2016)
Reference GFM: ITG-GRACE2010s (Mayer-Gürr et al., 2010)
Empirical Parameters: Daily constant-piecewise
Coord. Axis Combination: TBD
Single Sat. Combination: NEQ, equal weights
Temporal correlations: Empirical decorrelation filter
Drag Model: NRLMSISE (Picone et al., 2002)
EARP and EIRP Models: Knocke, Ries and Tapley (1988)
Non-tidal Model: AOD1B-RL06 (Dobslaw et al., 2017)
Atmospheric Tidal Model: Biancale and Bode (2006)
Ocean Tidal Model: FES2004 (Lyard et al., 2006)
Permanent Tide System: tide-free

B.3 Institute of Geodesy Graz

Software: Gravity Recovery Object Oriented Programming System (GROOPS) (Mayer-gürr et al., 2020)
Approach: Short-Arcs Approach (SAA) (Mayer-Gürr, 2006)
Reference GFM: GOCO05S (Mayer-Gürr, 2015)
Empirical Parameters: Piecewise linear for each arc (ranging from 15 to 45 minutes)
Coord. Axis Combination: TBD
Single Sat. Combination: NEQ, relative weighting from VCE
Temporal correlations: Empirical covariance function
Drag Model: JB2008 (Bowman et al., 2008)
EARP and EIRP Models: Rodriguez-Solano et al. (2012)
Non-tidal Model: AOD1B-RL06 (Dobslaw et al., 2017)
Atmospheric Tidal Model: Biancale and Bode (2006)
Ocean Tidal Model: FES2014 (Carrere et al., 2015)
Permanent Tide System: zero tide

B.4 Ohio State University

Software: (developed in-house)
Approach: Improved Energy Balance Approach (IEBA) (Shang et al., 2015)
Reference GFM: GIF48 (Ries et al., 2011) up to D/O 200
Empirical Parameters: 2nd order polynomial every 3 hours, 1-CPR sinusoidal every 24 hours

Coord. Axis Combination:	TBD
Single Sat. Combination:	NEQ, equal weights
Temporal correlations:	None
Drag Model:	NRLMSISE (Picone et al., 2002)
EARP and EIRP Models:	Knocke, Ries and Tapley (1988)
Non-tidal Model:	AOD1B (Flechtner, Schmidt and Meyer, 2006; Flechtner, 2007; Flechtner, 2011)
Atmospheric Tidal Model:	Biancale and Bode (2006)
Ocean Tidal Model:	EOT11a (Savcenko and Bosch, 2012)
Permanent Tide System:	tide-free

B.5 Institut für Geodäsie und Geoinformation

Software:	GROOPS
Approach:	Short-Arcs Approach (SAA) (Mayer-Gürr, 2006)
Reference GFM:	GOCO06S (Kvas et al., 2021)
Empirical Parameters:	**Drag + SRP + EIRP + EARP**: Bias per arc (45 minutes)
	Drag: Scale per arc (45 minutes) and direction
	SRP + EIRP + EARP: Scale per day
Single Sat. Combination:	NEQ, equal weights
Temporal correlations:	None
Drag Model:	NRLMSIS2 (Emmert et al., 2021)
SRP, EARP and EIRP Models:	Vielberg and Kusche (2020)
Non-tidal Model:	AOD1B-RL06 (Dobslaw et al., 2017)
Atmospheric Tidal Model:	AOD1B-RL06 (Dobslaw et al., 2017)
Ocean Tidal Model:	FES2014 (Carrere et al., 2015)
Permanent Tide System:	zero tide

B.6 Common

Regularization:	none
Solid Earth Tidal Model:	IERS2010
Pole Tidal Model:	IERS2010
Ocean Pole Tidal Model:	IERS2010
Third body perturbations:	Sun, Moon, Mercury, Venus, Mars, Jupiter and Saturn, following the JPL-PLE (Folkner et al., 2014)
$C_{2,0}$ **coefficient:**	estimated alongside other coefficients

Acronyms

AA	Acceleration Approach, Rummel (1979)
AIUB	Astronomical Institute of the University of Bern, Switzerland, `www.aiub.unibe.ch`
AIUB-GRACE03S	AIUB GRACE-only static model, version 3, Jäggi et al. (2011)
AOD1B	Atmosphere and Ocean De-aliasing Level 1B product, Flechtner, Schmidt and Meyer (2006), Flechtner (2007) and Flechtner (2011)
AOD1B-RL06	Atmosphere and Ocean De-aliasing Level 1B RL06 product, Dobslaw et al. (2017)
ASU	Astronomical Institute (Astronomický ústav), AVCR, Ondřejov, `www.asu.cas.cz/en`

AVCR	Czech Academy of Sciences (Akademie věd České Republiky), Czech Republic, `www.avcr.cz/en/`
CODE	Centre for Orbit Determination in Europe, Dach et al. (2017)
CMA	Celestial Mechanics Approach, Beutler et al. (2010)
CPR	Cycle Per Revolution
CSR	Center for Space Research, UT Austin, USA, `www.csr.utexas.edu`
D/O	Degree and Order
DAA	Decorrelated Acceleration Approach, Bezděk et al. (2014) and Bezděk et al. (2016)
EARP	Earth Albedo Radiation Pressure
EIRP	Earth Infrared Radiation Pressure
EBA	Energy Balance Approach, O'Keefe (1957) and Jekeli (1999)
EOT	Empirical Ocean Tide model
EOT11a	2011 Empirical Ocean Tide model, Savcenko and Bosch (2012)
EWH	Equivalent Water Height
EOP	Earth Orientation Parameter
ERP	Earth Rotation Parameters
FES	Finite Element Solution global tide model
FES2004	2004 Finite Element Solution global tide model, Lyard et al. (2006)
FES2014	2014 Finite Element Solution global tide model, Carrere et al. (2015)
GFM	Gravity Field Model
GIF48	GRACE Intermediate Field 48, Ries et al. (2011)
GNSS	Global Navigation Satellite System
GOCE	Gravity field and steady-state Ocean Circulation Explorer, Balmino et al. (1999) and Floberghagen et al. (2011)
GOCO	Gravity Observation COmbination
GOCO05S	GOCO release 05 satellite-only gravity field model, Mayer-Gürr (2015)
GOCO06S	GOCO release 06 satellite-only gravity field model, Kvas et al. (2021)
GPS	Global Positioning System
GRACE	Gravity Recovery And Climate Experiment, Tapley, Reigber and Melbourne (1996) and Tapley (2004)
GRACE-FO	GRACE Follow On, Kornfeld et al. (2019)
GROOPS	Gravity Recovery Object Oriented Programming System, Mayer-gürr et al. (2020)
GSFC	Goddard Space Flight Center, United States of America (USA), `www.nasa.gov/centers/goddard`
IAU	International Astronomical Union
IEBA	Improved Energy Balance Approach, Shang et al. (2015)
IERS	International Earth Rotation Service
IERS2010	IERS Conventions 2010, Petit and Luzum (2010)
IfG	Institute of Geodesy, TUG, Graz, `www.ifg.tugraz.at`
IGS	International GNSS Service, Dow, Neilan and Gendt (2005)
IGG	Institut für Geodäsie und Geoinformation, Germany, `www.igg.uni-bonn.de`
ITG	Institut für Geodäsie und Geoinformation, Germany www.igg.uni-bonn.de
ITG-GRACE2010s	ITG GRACE-only static model, 2010, Mayer-Gürr et al. (2010)
JB2008	Jacchia-Bowman 2008, Bowman et al. (2008)
JPL	Jet Propulsion Laboratory, USA, `www.jpl.nasa.gov`
JPL-PLE	JPL Planetary and Lunar Ephemerides, Folkner et al. (2014)
KO	Kinematic Orbit
L1B	Level 1B data

LAMBDA	Least-squares Ambiguity De-correlation Adjustment, Teunissen (1995)
LEO	Low-Earth Orbit
LS	least-squares
MLAMBDA	Modified LAMBDA method, Chang, Yang and Zhou (2005)
N/A	Not Applicable
NEQ	Normal Equation
NRLMSISE	US Naval Research Laboratory Mass Spectrometer and Incoherent Scatter radar atmospheric model, Picone et al. (2002)
NRLMSIS2	US Naval Research Laboratory Mass Spectrometer and Incoherent Scatter radar atmospheric model, version 2, Emmert et al. (2021)
OSU	Ohio State University, `www.osu.edu`
PCV	Phase Center Variation
POD	Precise Orbit Determination
PSO	Precise or Post-processed Science Orbit
RL06	Release 6
ROTI	Rate of TEC Index
RMS	Root Mean Squared
SAA	Short-Arcs Approach, Mayer-Gürr (2006)
SH	Spherical Harmonic
SLR	Satellite Laser Ranging, Smith and Turcotte (1993) and Combrinck (2010)
SNR	Signal-to-Noise Ratio
SRP	Solar Radiation Pressure
TEC	Total Electron Content
TU Delft	Delft University of Technology, Netherlands, `www.tudelft.nl`
TUG	Graz University of Technology, Austria, `www.tugraz.at`
UT Austin	University of Texas at Austin, `www.utexas.edu`
USA	United States of America
VCE	Variance Component Estimation
WP	Work Package

Symbols

C Stokes coefficient.

References

Balmino, G. et al. (1999). **The Four Candidate Earth Explorer Core Missions - Gravity Field and Steady-State Ocean Circulation Mission**. Tech. rep. SP- 1233(1). Noordwijk, The Netherlands: European Space Agency (cit. on p. 42).

Bettadpur, Srinivas et al. (2015). **Evaluation of the GGM05 Mean Earth Gravity Model**. In: *EGU General Assembly Conference Abstracts* 17, p. 4153 (cit. on p. 7).

Beutler, Gerhard et al. (2010). **The celestial mechanics approach: theoretical foundations**. In: *Journal of Geodesy* 84.10, pp. 605–624. DOI: `10.1007/s00190-010-0401-7` (cit. on pp. 39, 42).

Bezděk, Aleš et al. (2014). **Gravity field models from kinematic orbits of CHAMP, GRACE and GOCE satellites**. In: *Advances in Space Research* 53.3, pp. 412–429. DOI: `10.1016/j.asr.2013.11.031` (cit. on pp. 40, 42).

Bezděk, Aleš et al. (2016). **Time-variable gravity fields derived from GPS tracking of Swarm**. In: *Geophysical Journal International* 205.3, pp. 1665–1669. DOI: 10.1093/gji/ggw094 (cit. on pp. 6, 40, 42).

Biancale, R. and A. Bode (2006). **Mean annual and seasonal atmospheric tide models based on 3-hourly and 6-hourly ECMWF surface pressure data**. Tech. rep. Potsdam, Germany: Deutsches GeoForschungsZentrum GFZ. DOI: 10.2312/GFZ.b103-06011 (cit. on pp. 40, 41).

Bowman, Bruce et al. (2008). **A New Empirical Thermospheric Density Model JB2008 Using New Solar and Geomagnetic Indices**. In: *AIAA/AAS Astrodynamics Specialist Conference and Exhibit*. August. Reston, Virigina: American Institute of Aeronautics and Astronautics. DOI: 10.2514/6.2008-6438 (cit. on pp. 40, 42).

Carrere, L et al. (2015). **FES 2014, a new tidal model on the global ocean with enhanced accuracy in shallow seas and in the Arctic region**. In: *EGU General Assembly*. Vienna, Austria (cit. on pp. 40–42).

Chang, X. W., Xiaohua Yang and Tianyang Zhou (2005). **MLAMBDA: a modified LAMBDA method for integer least-squares estimation**. In: *Journal of Geodesy* 79.9, pp. 552–565. DOI: 10.1007/s00190-005-0004-x (cit. on pp. 39, 43).

Cheng, M. and John Ries (2018). **GRACE Technical Note 11: Monthly estimates of C20 from 5 satellites based on GRACE RL06 models**. Austin, USA. URL: https://podaac-tools.jpl.nasa.gov/drive/files/allData/grace/docs/TN-11_C20_SLR.txt (cit. on p. 7).

Combrinck, Ludwig (2010). **Satellite Laser Ranging**. In: *Sciences of Geodesy - I*. Ed. by Guochang Xu. Berlin, Heidelberg: Springer Berlin Heidelberg. Chap. 9, pp. 301–338. DOI: 10.1007/978-3-642-11741-1_9 (cit. on p. 43).

Coppola, Vincent, John H Seago and David A Vallado (2009). **The IAU 2000a and IAU 2006 Precession-Nutation theories and their implementations**. In: *Advances in the Astronautical Sciences* 09.159, pp. 1–20. URL: https://www.agi.com/getmedia/c85a440a-cf71-4e08-ad78-fa73736cee6c/Precession-nutation-Theories-and-their-Implementation.pdf (cit. on p. 39).

Dach, Rolf et al. (2015). **Bernese GNSS Software Version 5.2**. Bern: Bern Open Publishing. DOI: 10.7892/boris.72297 (cit. on pp. 38, 39).

Dach, Rolf et al. (2017). **CODE final product series for the IGS**. Bern, Switzerland. DOI: 10.7892/boris.75876.2 (cit. on pp. 38, 42).

Dobslaw, H. et al. (2017). **A new high-resolution model of non-tidal atmosphere and ocean mass variability for de-aliasing of satellite gravity observations: AOD1B RL06**. In: *Geophysical Journal International* 211.1, pp. 263–269. DOI: 10.1093/gji/ggx302 (cit. on pp. 40, 41).

Dow, J.M. M., R.E. E. Neilan and G. Gendt (2005). **The International GPS Service: Celebrating the 10th anniversary and looking to the next decade**. In: *Advances in Space Research* 36.3, pp. 320–326. DOI: 10.1016/j.asr.2005.05.125 (cit. on p. 42).

Emmert, J. T. et al. (2021). **NRLMSIS 2.0: A Whole-Atmosphere Empirical Model of Temperature and Neutral Species Densities**. In: *Earth and Space Science* 8.3. DOI: 10.1029/2020EA001321 (cit. on pp. 41, 43).

Flechtner, Frank (2007). **Gravity Recovery and Climate Experiment AOD1B Product Description Document for product releases 01 to 04**. Technical report GR-GFZ-AOD-0001. Potsdam: GeoForschungszentrum. URL: ftp://podaac.jpl.nasa.gov/pub/grace/doc/AOD1B_20070413.pdfhttps://www.gfz-potsdam.de/fileadmin/gfz/sec12/pdf/GRACE/AOD1B/AOD1B_20070413.pdf (cit. on pp. 40, 41).

Flechtner, Frank (2011). **GRACE AOD1B RL04 Quality Assurance**. Miscellaneous. URL: http://op.gfz-potsdam.de/grace/results/grav/g007_aod1b_rl04.html (visited on 23/07/2015) (cit. on pp. 40, 41).

Flechtner, Frank, Roland Schmidt and Ulrich Meyer (2006). **De-aliasing of Short-term Atmospheric and Oceanic Mass Variations for GRACE**. In: *Observation of the Earth System from Space*. Ed. by J. Flury et al. Springer Berlin Heidelberg, pp. 83–97. DOI: 10.1007/3-540-29522-4_7 (cit. on pp. 40, 41).

Floberghagen, Rune et al. (2011). **Mission design, operation and exploitation of the gravity field and steady-state ocean circulation explorer mission**. In: *Journal of Geodesy* 85.11, pp. 749–758. DOI: 10.1007/s00190-011-0498-3 (cit. on p. 42).

Folkner, William M et al. (2014). **The Planetary and Lunar Ephemerides DE430 and DE431**. In: *Interplanet. Netw. Prog. Rep* 42.196. URL: https://ipnpr.jpl.nasa.gov/progress_report/42-196/196C.pdf (cit. on pp. 41, 42).

Guo, J. Y., X. J. Duan and C. K. Shum (2010). **Non-isotropic Gaussian smoothing and leakage reduction for determining mass changes over land and ocean using GRACE data**. In: *Geophysical Journal International* 181.1, pp. 290–302. DOI: 10.1111/j.1365-246X.2010.04534.x (cit. on p. 8).

Guo, J. Y. et al. (2015). **On the energy integral formulation of gravitational potential differences from satellite-to-satellite tracking**. In: *Celestial Mechanics and Dynamical Astronomy* 121.4, pp. 415–429. DOI: 10.1007/s10569-015-9610-y (cit. on p. 6).

Helleputte, T. van (2004). **GPS High Precision Orbit Determination Software Tools: User Manual**. Oberpfaffenhofen (cit. on p. 37).

Hoque, M. Mainul and N. Jakowski (2008). **Estimate of higher order ionospheric errors in GNSS positioning**. In: *Radio Science* 43.5, n/a–n/a. DOI: 10.1029/2007RS003817 (cit. on p. 39).

Jäggi, A. et al. (2011). **AIUB-GRACE03S**. Bern, Switzerland. URL: http://icgem.gfz-potsdam.de/ (cit. on pp. 39, 41).

Jäggi, A. et al. (2016). **Swarm kinematic orbits and gravity fields from 18 months of GPS data**. In: *Advances in Space Research* 57.1, pp. 218–233. DOI: 10.1016/j.asr.2015.10.035 (cit. on p. 6).

Jekeli, Christopher (1999). **The determination of gravitational potential differences from satellite-to-satellite tracking**. In: *Celestial Mechanics and Dynamical Astronomy* 75.2, pp. 85–101. DOI: 10.1023/A:1008313405488 (cit. on p. 42).

Knocke, P., J. Ries and B. Tapley (1988). **Earth radiation pressure effects on satellites**. In: *Astrodynamics Conference*. Reston, Virigina: American Institute of Aeronautics and Astronautics. DOI: 10.2514/6.1988-4292 (cit. on pp. 40, 41).

Kornfeld, Richard P. et al. (2019). **GRACE-FO: The Gravity Recovery and Climate Experiment Follow-On Mission**. In: *Journal of Spacecraft and Rockets* 56.3, pp. 931–951. DOI: 10.2514/1.A34326 (cit. on p. 42).

Kouba, J. (2009). **A simplified yaw-attitude model for eclipsing GPS satellites**. In: *GPS Solutions* 13.1, pp. 1–12. DOI: 10.1007/s10291-008-0092-1 (cit. on p. 39).

Kvas, Andreas et al. (2021). **GOCO06s – a satellite-only global gravity field model**. In: *Earth System Science Data* 13.1, pp. 99–118. DOI: 10.5194/essd-13-99-2021 (cit. on pp. 41, 42).

Lieske, J H et al. (1977). **Expression for the precession quantities based upon the IAU (1976) system of astronomical constants**. In: *Astronomy and Astrophysics* 58, pp. 1–16 (cit. on p. 38).

Loomis, B. D., K. E. Rachlin and S. B. Luthcke (2019). **Improved Earth Oblateness Rate Reveals Increased Ice Sheet Losses and Mass-Driven Sea Level Rise**. In: *Geophysical Research Letters* 46.12, pp. 6910–6917. DOI: 10.1029/2019GL082929 (cit. on p. 7).

Loomis, B.D. and K.E. Rachlin (2020). **GRACE Technical Note 14: NASA GSFC SLR C20 and C30 solutions**. Greenbelt, USA. URL: https://podaac-tools.jpl.nasa.gov/drive/files/allData/gracefo/docs/TN-14_C30_C20_GSFC_SLR.txt (cit. on p. 7).

Lyard, Florent et al. (2006). **Modelling the global ocean tides: modern insights from FES2004**. In: *Ocean Dynamics* 56.5-6, pp. 394–415. DOI: 10.1007/s10236-006-0086-x (cit. on pp. 40, 42).

Mayer-Gürr, Torsten (2006). **Gravitationsfeldbestimmung aus der Analyse kurzer Bahnbögen am Beispiel der Satellitenmissionen CHAMP und GRACE**. PhD thesis. Rheinischen Friedrich-Wilhelms Universität Bonn. URL: http://hss.ulb.uni-bonn.de/2006/0904/0904.pdf (cit. on pp. 40, 41, 43).

— (2015). **The Combined Satellite Gravity Field Model GOCO05s**. In: *EGU General Assembly*. EGU2015-12364. Vienna, Austria (cit. on pp. 40, 42).

Mayer-Gürr, Torsten et al. (2010). **ITG-Grace2010: the new GRACE gravity field release computed in Bonn**. In: *EGU General Assembly*. EGU2010-2446. Vienna, Austria. URL: http://www.igg.uni-bonn.de/apmg/index.php?id=itg-grace2010 (cit. on pp. 40, 42).

Mayer-gürr, Torsten et al. (2020). **GROOPS : A software toolkit for gravity field recovery and GNSS processing**. In: *Earth and Space Science Open Archive*. DOI: 10.1002/essoar.10505041.1 (cit. on pp. 38, 40, 42).

O'Keefe, John A. (1957). **An application of Jacobi's integral to the motion of an earth satellite**. In: *The Astronomical Journal* 62, p. 265. DOI: 10.1086/107530 (cit. on p. 42).

Petit, Gérard Gerard and Brian Luzum (2010). **IERS Conventions (2010)**. Frankfurt am Main. URL: http://www.iers.org/TN36/ (cit. on pp. 38, 39, 42).

Picone, J. M. et al. (2002). **NRLMSISE-00 empirical model of the atmosphere: Statistical comparisons and scientific issues**. In: *Journal of Geophysical Research: Space Physics* 107.A12, SIA 15–1–SIA 15–16. DOI: 10.1029/2002JA009430 (cit. on pp. 40, 41, 43).

Rebischung, P and R Schmid (2016). **IGS14/igs14.atx: a new Framework for the IGS Products**. In: *AGU Fall Meeting Abstracts*. Vol. 2016, G41A–0998 (cit. on p. 38).

Ries, John C. et al. (2011). **Mean Background Gravity Fields for GRACE processing**. In: *GRACE Science Team Meeting*. Austin, USA. URL: http://download.csr.utexas.edu/pub/grace/Proceedings/Presentations_GSTM2011.pdf (cit. on pp. 40, 42).

Rodriguez-Solano, C. J. et al. (2012). **Impact of Earth radiation pressure on GPS position estimates**. In: *Journal of Geodesy* 86.5, pp. 309–317. DOI: 10.1007/s00190-011-0517-4 (cit. on p. 40).

Rummel, R. (1979). **Determination of short-wavelength components of the gravity field from satellite-to-satellite tracking or satellite gradiometry**. In: *Manuscripta Geodaetica* 4.2, pp. 107–148 (cit. on p. 41).

Savcenko, R and W Bosch (2012). **EOT11a - Empirical ocean tide model from multi-mission satellite altimetry**. Tech. rep. München, Germany: Deutsches Geodätisches Forschungsinstitut. URL: https://epic.awi.de/36001/1/DGFI_Report_89.pdf (cit. on pp. 40–42).

Schmid, Ralf et al. (2007). **Generation of a consistent absolute phase-center correction model for GPS receiver and satellite antennas**. In: *Journal of Geodesy* 81.12, pp. 781–798. DOI: 10.1007/s00190-007-0148-y (cit. on p. 38).

Seidelmann, P. K. (1982). **1980 IAU Theory of Nutation: The final report of the IAU Working Group on Nutation**. In: *Celestial Mechanics* 27.1, pp. 79–106. DOI: 10.1007/BF01228952 (cit. on p. 38).

Shang, Kun et al. (2015). **GRACE time-variable gravity field recovery using an improved energy balance approach**. In: *Geophysical Journal International* 203.3, pp. 1773–1786. DOI: 10.1093/gji/ggv392 (cit. on pp. 40, 42).

Smith, David E. and Donald L. Turcotte (1993). **Millimeter Accuracy Satellite Laser Ranging: a Review**. In: *Contributions of Space Geodesy to Geodynamics: Technology*. Ed. by John J. Degnan. Vol. 25. Geodynamics Series. Washington, D. C.: American Geophysical Union. DOI: 10.1029/GD025p0133 (cit. on p. 43).

Tapley, B., C. Reigber and W Melbourne (1996). **Gravity Recovery And Climate Experiment (GRACE) mission**. Baltimore, USA (cit. on p. 42).

Tapley, Byron D. (2004). **GRACE Measurements of Mass Variability in the Earth System**. In: *Science* 305.5683, pp. 503–505. DOI: 10.1126/science.1099192 (cit. on p. 42).

Teixeira da Encarnação, João and Pieter Visser (2017). **TN-01 : Standards and Background Models**. Tech. rep. Delft, the Netherlands: Delft University of Technology. DOI: 10.13140/RG.2.2.12840.32006/1 (cit. on p. 6).

— (2019). **TN-03: Swarm models validation**. Tech. rep. TU Delft. DOI: 10.13140/RG.2.2.33313.76640 (cit. on p. 6).

Teunissen, P. J. G. (1995). **The least-squares ambiguity decorrelation adjustment: a method for fast GPS integer ambiguity estimation**. In: *Journal of Geodesy* 70.1-2, pp. 65–82. DOI: 10.1007/BF00863419 (cit. on p. 43).

Vielberg, Kristin and Jürgen Kusche (2020). **Extended forward and inverse modeling of radiation pressure accelerations for LEO satellites**. In: *Journal of Geodesy* 94.4, p. 43. DOI: 10.1007/s00190-020-01368-6 (cit. on p. 41).

Wermuth, Martin, Oliver Montenbruck and Tom Van Helleputte (2010). **GPS high precision orbit determination software tools (GHOST)**. In: *4th International Conference on Astrodynamics Tools and Techniques*. Madrid: ESA WPP-308 (cit. on p. 37).

Zehentner, Norbert (2016). **Kinematic orbit positioning applying the raw observation approach to observe time variable gravity**. Doctoral Dissertation. Graz University of Technology, p. 175. DOI: 10.13140/RG.2.2.33916.33927 (cit. on p. 39).

Zehentner, Norbert and Torsten Mayer-Gürr (2016). **Precise orbit determination based on raw GPS measurements**. In: *Journal of Geodesy* 90.3, pp. 275–286. DOI: 10.1007/s00190-015-0872-7 (cit. on p. 6).